Caenorhabditis elegans HOPS and CCZ-1 mediate trafficking to lysosome-related organelles independently of RAB-7 and SAND-1

Jared L. Delahaye[a], Olivia K. Foster[b], Annalise Vine[b], Daniel S. Saxton[a], Thomas P. Curtin[b], Hannah Somhegyi[a], Rebecca Salesky[a], and Greg J. Hermann[a,b]
[a]Department of Biology and [b]Program in Biochemistry and Molecular Biology, Lewis & Clark College, Portland, OR 97219

ABSTRACT **As early endosomes mature, the SAND-1/CCZ-1 complex acts as a guanine nucleotide exchange factor (GEF) for RAB-7 to promote the activity of its effector, HOPS, which facilitates late endosome–lysosome fusion and the consumption of AP-3–containing vesicles. We show that CCZ-1 and the HOPS complex are essential for the biogenesis of gut granules, cell type–specific, lysosome-related organelles (LROs) that coexist with conventional lysosomes in *Caenorhabditis elegans* intestinal cells. The HOPS subunit VPS-18 promotes the trafficking of gut granule proteins away from lysosomes and functions downstream of or in parallel to the AP-3 adaptor. CCZ-1 also acts independently of AP-3, and *ccz-1* mutants mistraffic gut granule proteins. Our results indicate that SAND-1 does not participate in the formation of gut granules. In the absence of RAB-7 activity, gut granules are generated; however, their size and protein composition are subtly altered. These observations suggest that CCZ-1 acts in partnership with a protein other than SAND-1 as a GEF for an alternate Rab to promote gut granule biogenesis. Point mutations in GLO-1, a Rab32/38-related protein, predicted to increase spontaneous guanine nucleotide exchange, specifically suppress the loss of gut granules by *ccz-1* and *glo-3* mutants. GLO-3 is known to be required for gut granule formation and has homology to SAND-1/Mon1–related proteins, suggesting that CCZ-1 functions with GLO-3 upstream of the GLO-1 Rab, possibly as a GLO-1 GEF. These results support LRO formation occurring via processes similar to conventional lysosome biogenesis, albeit with key molecular differences.**

Monitoring Editor
Francis A. Barr
University of Oxford

Received: Sep 10, 2013
Revised: Jan 22, 2014
Accepted: Jan 24, 2014

INTRODUCTION

Many cell types contain multiple types of lysosomal compartments. Like the ubiquitous conventional lysosomes with which they typically coexist, lysosome-related organelles (LROs) are often acidified and produced through the action of the endocytic pathway (Marks *et al.*, 2013; Yousefian *et al.*, 2013). LROs represent a diverse array of compartments that are distinguished from each other by their cell type–specific morphology, composition, and function (Dell'Angelica *et al.*, 2000). Defective formation of LROs can lead to the disease Hermansky–Pudlak syndrome (HPS). HPS patients and mouse HPS disease models have altered body pigmentation and blood clotting, resulting from aberrant biogenesis of LROs in melanocytes and platelets (Huizing *et al.*, 2008). LROs are not restricted to vertebrates and are found in invertebrates, protozoa, and possibly plants (Raposo *et al.*, 2007; Sohn *et al.*, 2007; Docampo *et al.*, 2010).

Gut granules are cell type–specific LROs found within *Caenorhabditis elegans* intestinal cells (Hermann *et al.*, 2005). They contain birefringent and autofluorescent material, whose accumulation is coincident with their formation during embryogenesis (Laufer *et al.*, 1980; Bossinger and Schierenberg, 1992). Gut granules function in zinc storage, limiting its toxicity (Roh *et al.*, 2012), contain tryptophan

This article was published online ahead of print in MBoC in Press (http://www.molbiolcell.org/cgi/doi/10.1091/mbc.E13-09-0521) on February 5, 2014.

Address correspondence to: Greg J. Hermann (hermann@lclark.edu).

Abbreviations used: GEF, guanine nucleotide exchange factor; GFP, green fluorescent protein; Glo, gut granule loss; HPS, Hermansky–Pudlak syndrome; LRO, lysosome-related organelle; SNARE, soluble *N*-ethylmaleimide–sensitive factor attachment protein receptor.

derivatives of the kynurenine pathway (Coburn *et al.*, 2013), and are linked to lipid metabolism (Mak *et al.*, 2006; O'Rourke *et al.*, 2009; O'Rourke and Ruvkun, 2013). Although gut granules share some characteristics and proteins with conventional lysosomes, the two organelles are distinct and coexist within intestinal cells (Clokey and Jacobson, 1986; Levitte *et al.*, 2010; Hermann *et al.*, 2012). Many of the factors mediating trafficking to *C. elegans* gut granules have evolutionarily conserved roles in the biogenesis of LROs in *Drosophila* and mammals (Hermann *et al.*, 2005, 2012; Raposo *et al.*, 2007).

Most of the molecular machinery known to guide LRO biogenesis is also used in the formation of conventional lysosomes. These include the AP-3 adaptor (Dell'Angelica, 2009), BLOC-1 (Di Pietro *et al.*, 2006; Salazar *et al.*, 2006; Setty *et al.*, 2007), and HOPS tethering complexes (Zlatic *et al.*, 2011a; Solinger and Spang, 2013), suggesting that the mechanisms promoting trafficking to LROs and lysosomes are likely to be similar. However, there are some factors, such as Rab32/38-related proteins (Ma *et al.*, 2004; Hermann *et al.*, 2005; Wasmeier *et al.*, 2006), that likely function exclusively in the biogenesis of LROs. Knowing the similarities and differences between trafficking pathways leading to lysosomes and LROs will be key in understanding the biogenesis of LROs and the cellular processes that simultaneously generate these related, yet structurally and functionally distinct organelles.

Studies reveal an evolutionarily conserved mechanism for protein trafficking from early endosomes to lysosomes by which early endosomes, or early endosome subdomains (Rink *et al.*, 2005; Vonderheit and Helenius, 2005), mature into late endosomes via the action of a SAND-1(Mon1)/CCZ-1 complex. This complex promotes both the inactivation and removal of RAB5 from early endosomes and the activation and recruitment of RAB7, a process called Rab conversion (Kinchen and Ravichandran, 2010; Nordmann *et al.*, 2010; Poteryaev *et al.*, 2010; Gerondopoulos *et al.*, 2012). Active RAB7 recruits the HOPS tethering complex to late endosomes and lysosomes (Cabrera *et al.*, 2010; Ostrowicz *et al.*, 2010), promoting their heterotypic fusion to create endolysosomes (Caplan *et al.*, 2001; Sriram *et al.*, 2003; Richardson *et al.*, 2004; Kinchen *et al.*, 2008; Hickey and Wickner, 2010; Pols *et al.*, 2013), which then mature into lysosomes via membrane budding (Pryor *et al.*, 2000; Bright *et al.*, 2005). HOPS also functions in the fusion of Golgi apparatus or early endosome–derived, AP-3–containing vesicles with endolysosomes and lysosomes (Darsow *et al.*, 2001; Angers and Merz, 2009; Cabrera *et al.*, 2010).

Parallels with lysosome biogenesis suggest that similar mechanisms function in trafficking to LROs. Mammalian paralogues of SAND-1 and CCZ-1, called HPS1 and HPS4 (Hoffman-Sommer *et al.*, 2005; Kinch and Grishin, 2006), respectively, form BLOC-3 (Chiang *et al.*, 2003; Martina *et al.*, 2003; Nazarian *et al.*, 2003), which functions in the formation of LROs (Oh *et al.*, 1996; Suzuki *et al.*, 2002). Rab7 is localized on immature and mature LROs (Jordens *et al.*, 2006; Zhang *et al.*, 2011; Ambrosio *et al.*, 2012), and disrupting Rab7 activity can alter the distribution of LRO contents (Hirosaki *et al.*, 2002; Kawakami *et al.*, 2008; Hida *et al.*, 2011). In various metazoan systems, mutations affecting the function of HOPS subunits cause reduced numbers of LROs (Sevrioukov *et al.*, 1999; Hermann *et al.*, 2005; Pulipparacharuvil *et al.*, 2005; Sadler *et al.*, 2005; Maldonado *et al.*, 2006; Akbar *et al.*, 2009; Thomas *et al.*, 2011). AP-3 functions during the formation of LROs (Ooi *et al.*, 1997; Simpson *et al.*, 1997; Kantheti *et al.*, 1998; Dell'Angelica *et al.*, 1999; Feng *et al.*, 1999; Mullins *et al.*, 1999, 2000; Kretzschmar *et al.*, 2000; Hermann *et al.*, 2005) by interacting with the cytoplasmic domain of a subset of LRO-destined transmembrane proteins, directing their vesicular transport to LROs from early endosomes (Huizing *et al.*, 2001; Theos *et al.*, 2005; Setty *et al.*, 2007).

Here we systematically analyze the role of genes promoting protein trafficking from early endosomes to lysosomes during gut granule biogenesis in *C. elegans* intestinal cells and document genetic interactions revealing their functional relationships. Our results suggest that the pathways constructing LROs and conventional lysosomes are likely similar; however, they highlight significant molecular differences.

RESULTS

Formation of autofluorescent and birefringent gut granules in endolysosomal trafficking mutants

To address whether the machinery that mediates protein trafficking from early endosomes to conventional lysosomes also affects trafficking to LROs, we used *C. elegans* mutants that lack or have strongly reduced activity of VPS-C/HOPS, CCZ-1, SAND-1/Mon1, and RAB-7. These mutants were analyzed for their effects on the formation of gut granules, which contain birefringent material and autofluorescent material and are acidified (Laufer *et al.*, 1980; Clokey and Jacobson, 1986; Bossinger and Schierenberg, 1992). Defective gut granule biogenesis leads to loss of acidified intestinal organelles and loss and/or extracellular misaccumulation of the birefringent and autofluorescent material, which we refer to as a gut granule loss (Glo) phenotype (Hermann *et al.*, 2005). Following standard *C. elegans* nomenclature, genes are given in lowercase italics and proteins are given in uppercase nonitalic.

VPS-C/HOPS. VPS-C comprises VPS-11, -16, -18, and -33. Two additional subunits, VPS-39 and -41, associate with VPS-C to form HOPS (Nickerson *et al.*, 2009; Balderhaar and Ungermann, 2013; Graham *et al.*, 2013). *C. elegans* encodes a protein orthologous to each HOPS subunit (Solinger and Spang, 2013; Supplemental Figure S1), and there are mutants predicted to severely disrupt the function of each of the six HOPS subunits (Supplemental Figure S1). Our prior work showed that mutations disrupting *vps-16* or *vps-41* led to a Glo phenotype in adults (Hermann *et al.*, 2005), and we found that additional mutant alleles and RNA interference (RNAi) targeting these genes led to a similar phenotype, further supporting their role in gut granule biogenesis (Figure 1 and Table 1). We investigated whether the four other subunits of VPS-C/HOPS were similarly required for gut granule biogenesis. Mutations in three other HOPS genes—*vps-11*, *vps33.1*, and *vps-39*—also led to a reduction in the number of autofluorescent compartments (Figure 1 and Table 1). Of these, *vps-39* presented the weakest Glo phenotype, which was enhanced by *vps-39(RNAi)* (Table 1), suggesting that the *vps-39* mutant allele retains function or the adult Glo phenotype can be maternally rescued. The *vps-18(tm1125)* mutant did not display an obvious alteration in adult gut granule number (Figure 1 and Table 1), although it did exhibit defective formation of gut granules in embryos (see later discussion).

The VPS-C/HOPS subunit mutants that exhibited an adult Glo phenotype also displayed maternal effect embryonic lethality, producing progeny that arrest at a stage in embryogenesis before the formation of gut granules, thus preventing an analysis of their effect on gut granules biogenesis in embryos (unpublished observations). We therefore used RNAi, which often leads to a partial knockdown of gene function, to assess the role of VPS-C/HOPS genes in embryonic gut granule biogenesis. Birefringent material, which can be visualized with polarization microscopy, is restricted to, and first becomes apparent within, gut granules at the bean stage, midway through embryogenesis (Laufer *et al.*, 1980). This marker continues

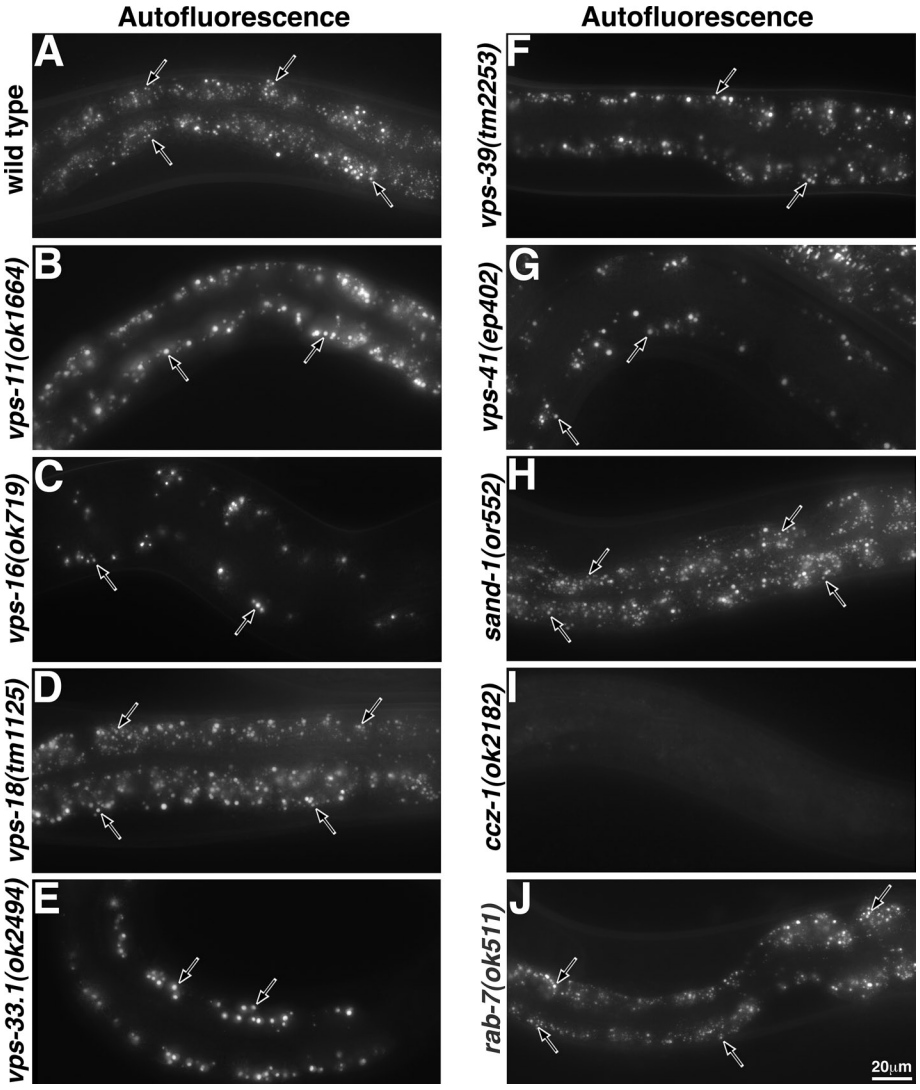

FIGURE 1: Autofluorescent compartments in adult intestinal cells. The 9-μm maximum-intensity projections, which span 50% the width of the intestine, of GFP channel autofluorescence centered on the lumen of the anterior intestine show that, in comparison to (A) wild type, the (B) *vps-11*, (C) *vps-16*, (E) *vps-33*, (F) *vps-39*, (G) *vps-41*, and (I) *ccz-1* mutants exhibited reduced numbers of autofluorescent compartments. Mutations in (D) *vps-18*, (H) *sand-1*, and (J) *rab-7* did not obviously alter the number of autofluorescent organelles. Black arrows denote representative autofluorescent compartments.

to specifically accumulate in gut granules as embryos elongate through the 1.5-fold to the pretzel stage (Hermann *et al.*, 2005; Figure 2A). We found that RNAi targeting *vps-11*, *-16*, *-33.1*, *-39*, and *41* led to an embryonic Glo phenotype (Figure 2, K–O, and Table 2).

The *vps-18(tm1125)* mutant, in contrast to other VPS-C/HOPS mutants, is temperature sensitive for growth, being viable between 15 and 22°C and displaying embryonic lethality at 25°C (Xiao *et al.*, 2009). This allele leads to temperature-sensitive defects in cell corpse degradation due to inhibition of lysosome formation and function (Xiao *et al.*, 2009). *vps-18* mutant adults did not display a significant Glo phenotype at any temperature (Figure 1D and Table 1). They do, however, show temperature-sensitive defects in the formation of embryonic gut granules (Figure 2E and Table 2). At 15°C, pretzel-stage *vps-18* mutant embryos displayed a weak Glo phenotype (Table 2 and Figure 2P). At 22°C, *vps-18* mutant embryos displayed a strong and fully penetrant Glo phenotype (Table 2 and Figure 2E), which was rescued by the introduction of *vps-18(+)::gfp* (Table 2). At 25°C, many *vps-18* mutant embryos arrested before elongation, and 76% (n = 33) of these contained birefringent material distributed throughout the embryo (Figure 2Q), suggestive of altered formation or trafficking of birefringent material, which is normally restricted to intestinal cells (Hermann *et al.*, 2005).

We carried out temperature-shift experiments to determine when *vps-18* activity promotes the formation of birefringent gut granules. *vps-18* mutant embryos cultured at the permissive temperature were shifted to the nonpermissive temperature during early to mid embryogenesis and then scored for the presence and localization of birefringent material at the pretzel stage. Consistent with VPS-18 functioning directly in the formation of gut granules, we found that nearly all of the *vps-18* mutant embryos upshifted before the early bean stage, when birefringent gut granules first become apparent (Laufer *et al.*, 1980), lacked or displayed a significant reduction in the number of birefringent intestinal granules (Figure 2R).

The *vps-18(tm1125)* allele introduces a premature stop codon predicted to truncate the C-terminal 760 amino acids of VPS-18, which contains the α-solenoid, coiled-coil, and RING finger domains (Xiao *et al.*, 2009; Supplemental Figure 1), suggesting that this allele may completely disrupt *vps-18(+)* activity. However, we found that application of *vps-18* RNAi to *vps-18(tm1125)* mutants led to a significant decrease in the number of autofluorescent granules (Table 1). Thus the *vps-18(tm1125)* mutant allele exhibits significant activity in promoting adult gut granule formation. In contrast, *vps-18(tm1125)* mutant embryos exhibited a fully penetrant Glo phenotype at 22°C (Table 2), suggesting that *vps-18* function is severely reduced at this stage. We therefore carried out our analyses of *vps-18* activity in embryos.

We first addressed whether the defect in gut granule formation exhibited by the *vps-18* mutant extended beyond just the generation and localization of birefringent material. Gut granules are the major acidified compartments within embryonic intestinal cells and are stained by LysoSensor Green, whose accumulation and fluorescence depend on an acidic pH (Levitte *et al.*, 2010). Whereas LysoSensor Green marked wild-type gut granules, organelles within *vps-18* mutant intestinal cells were not stained, indicating a general defect in gut granule biogenesis (Figure 2, F and J).

In metazoans, there are alternate VPS-16 and VPS-33 subunits that associate with VPS-C/HOPS (Zlatic *et al.*, 2011a; Solinger and Spang, 2013), which are necessary for the formation of some LROs (Lo *et al.*, 2005; Urban *et al.*, 2012). In *C. elegans*, SPE-39 is homologous to VPS-16, and VPS-33.2 and VPS-45 are homologous to VPS-33.1 (Solinger and Spang, 2013). Mutations in *spe-39* or *vps-45* and RNAi targeting *spe-39*, *vps-33.2*, or *vps-45* did not

Genotype	Percentage of animals with the specified number of autofluorescent organelles in anterior intestinal cells						*n*
	0	1–20	21–50	51–100	101–200	>200	
Wild type[a]	0	0	0	0	0	100	38
VPS-C subunits							
vps-11(ok1664)	0	0	0	76	24	0	34
vps-16(ok719)	0	13	87	0	0	0	31
vps-16(ok776)	0	4	92	4	0	0	25
vps-16(RNAi)[b]	0	3	41	56	0	0	87
spe-39(eb9)	0	0	0	0	0	100	25
spe-39(RNAi)[b]	0	0	0	0	8	92	25
vps-18(tm1125), 22°C	0	0	0	0	0	100	37
vps-18(tm1125), 25°C	0	0	0	0	59	41	22
vps-18(RNAi)[b]	0	0	0	0	8	92	25
vps-18(tm1125); vps-18(RNAi)	0	0	19	62	19	0	21
vps-33.1(ok2494)	0	4	81	15	0	0	26
vps-33.2(RNAi)[b]	0	0	0	0	15	85	48
vps-45(tm246)[c]	0	0	0	0	0	100	22
vps-45(RNAi)[b]	0	0	0	0	0	100	31
CORVET-specific subunit							
vps-8(RNAi)[b]	0	0	0	0	14	88	44
HOPS-specific subunits							
vps-39(ok2442)	0	0	0	10	84	6	31
vps-39(tm2253)	0	0	0	10	90	0	31
vps-39(RNAi)[b]	0	0	0	0	46	54	37
vps-39(tm2253); vps-39(RNAi)[d]	0	33	67	0	0	0	21
vps-41(ep402)	0	0	64	36	0	0	22
vps-41(ok3433)	0	0	21	75	4	0	44
vps-41(RNAi)[b]	0	60	40	0	0	0	30
HOPS regulators							
ccz-1(ok2182)	59	29	6	2	0	4	51
ccz-1(t2129)[d]	0	94	6	0	0	0	45
ccz-1(t2129) +ccz-1::yfp[e]	0	0	0	70	30	0	20
ccz-1(RNAi)[f]	0	0	0	5	90	5	21
sand-1(ok1963)	0	0	0	0	0	100	38
sand-1(or552)	0	0	0	0	0	100	25
HOPS interactors							
apt-6(ok429)	0	72	25	3	0	0	32
apt-7(tm920)	0	83	17	0	0	0	30
arl-8(tm2504)[g]	0	0	0	0	0	100	20
rab-7(ok511)[h]	0	0	0	0	0	100	23
rab-7(RNAi)[i]	0	0	0	0	0	100	25
Double mutants							
apt-6(ok429); vps-18(tm1125)[j]	100	0	0	0	0	0	45
apt-7(tm920); vps-18(tm1125)[j]	92	8	0	0	0	0	52

TABLE 1: Gut granules in adults.

Continues

Genotype	Percentage of animals with the specified number of autofluorescent organelles in anterior intestinal cells						n
	0	1–20	21–50	51–100	101–200	>200	
apt-6(ok429); vps-41(ep402)[k]	3	95	2	0	0	0	42
apt-6(ok429); ccz-1(RNAi)	75	25	0	0	0	0	20
apt-7(tm920); ccz-1(RNAi)	95	5	0	0	0	0	22
apt-7(tm920); ccz-1(ok2182)	100	0	0	0	0	0	25
apt-6(ok429); rab-7(ok511)[l]	0	50	50	0	0	0	24
apt-7(tm920); rab-7(ok511)[l]	0	62	38	0	0	0	21
apt-6(ok429); rab-7(RNAi)[l]	0	71	29	0	0	0	21
apt-7(tm920); rab-7(RNAi)[l]	0	87	13	0	0	0	23
apt-7(tm920); sand-1(or552)	0	96	4	0	0	0	28
glo-2(zu455)	0	46	54	0	0	0	63
glo-2(zu455); rab-7(ok511)[l]	0	52	48	0	0	0	27
glo-2(tm592)	0	0	0	31	69	0	29
glo-2(tm592); rab-7(ok511)[l]	0	0	0	41	59	0	22
glo-3(kx90)	0	33	67	0	0	0	21
glo-3(kx90); rab-7(ok511)[l]	3	90	7	0	0	0	30
pgp-2(kx48)	0	0	0	60	40	0	20
pgp-2(kx48); rab-7(ok511)[l]	0	27	73	0	0	0	30

All strains were grown at 22°C unless otherwise noted. Adult-stage animals were analyzed using fluorescence microscopy with a GFP or DAPI filter set and were scored for the number of autofluorescent organelles within the anterior intestine located between the pharynx and vulva.
[a]Wild type had >200 at both 22 and 25°C.
[b]RNAi was carried out in the *rrf-3(pk1426)* RNAi–sensitive strain (Simmer *et al.*, 2003). F33E2.4(RNAi) targeting a gene not involved in gut granule formation did not alter number of autofluorescent compartments in *rrf-3(-)*.
[c]*vps-45(tm246)* animals were grown at 22°C from early larvae to adulthood before scoring.
[d]*vps-39(tm2253)/nT1[qIs51]* animals were placed on RNAi plates as embryos and grown for two generations before being scored. Only animals lacking GFP, which are *vps-39(-)/vps-39(-)*, were analyzed. F33E2.4(RNAi) targeting a gene not involved in gut granule formation did not alter number of autofluorescent compartments in these animals (unpublished data).
[e]Dpy progeny of *dpy-11(e224) ccz-1(t2129)/nT1[qIs51]* were scored. *dpy-11(e224) ccz-1(t2129); jcpEx2[ccz-1::yfp; myo-2::gfp]* animals expressing GFP were scored. Non–GFP-expressing animals, which lack *jcpEx2*, were Glo (unpublished data).
[f]RNAi was carried out in the N2 background. F33E2.4(RNAi) targeting a gene not involved in gut granule formation did not alter number of autofluorescent compartments.
[g]Non–GFP-expressing *arl-8(-)/arl-8(-)* progeny of *arl-8(tm2504)/nT1[qIs51]* were scored.
[h]Non–GFP-expressing *rab-7(-)/rab-7(-)* progeny of *rab-7(ok511)/mIn1[mIs14]* were scored.
[i]Adults scored had prominent, enlarged, refractile structures visible with DIC microscopy in the most proximal oocytes, which are indicative of *rab-7(-)*.
[j]*unc-4(e120)*, which did not alter the Glo phenotype, was present in the background.
[k]*vps-41(-)/vps-41(-)* adult progeny of *vps-41(-)/+; apt-6(-)/apt-6(-)* parents were identified by the accumulation of apoptotic corpses in the germline and arrested embryos in the uterus.
[l]*rab-7(-)/rab-7(-)* adult progeny of *rab-7(-)/+; glo(-)/glo(-)* parents were identified by the refractile structures visible with DIC microscopy in the most proximal oocytes, which are indicative of *rab-7(-)*.

TABLE 1: Gut granules in adults. Continued

lead to an adult Glo phenotype (Table 1). The Arf-like GTPase Arl8 physically interacts with VPS41 in mammals, and mutation of the *C. elegans* orthologue *arl-8* phenocopies *vps-18* mutants (Xiao *et al.*, 2009; Nakae *et al.*, 2010; Garg *et al.*, 2011), suggesting that it functions with the HOPS complex. However, we did not see any effect of an *arl-8* mutation on the formation of autofluorescent gut granules (Table 1). In yeast, the VPS-C subunits can also associate with VPS-3 and VPS-8, instead of VPS-39 and VPS-41, to generate CORVET (Peplowska *et al.*, 2007). There is no obvious VPS-3 homologue in *C. elegans* (Solinger and Spang, 2013). Mutations or RNAi targeting *vps-8*/(*C42C1.4)* did not lead to a Glo phenotype (Tables 1 and 2). On the basis of the genes exhibiting a Glo phenotype when altered by mutation or targeted by RNAi, we conclude that the canonical HOPS complex, rather than the CORVET or a VPS-C/HOPS subcomplex, functions in the formation of gut granules.

sand-1/Mon1 and ccz-1. Current models for membrane trafficking to conventional lysosomes in *C. elegans* point to a role for a complex of SAND-1 and CCZ-1 as regulators of early endosome–to–late endosome maturation and RAB-5–to–RAB-7 conversion (Kinchen and Ravichandran, 2010; Nieto *et al.*, 2010; Poteryaev *et al.*, 2010). Mammalian genomes encode three distinct proteins—Mon1a, Mon1b, and HPS1—that are homologous to SAND-1 and two distinct proteins—Ccz1 and HPS4—that are homologous to CCZ-1. HPS1 and HPS4 function in the formation of LROs (Oh *et al.*, 1996; Suzuki *et al.*, 2002). The genome of *C. elegans* encodes only single proteins that are highly homologous to SAND-1/Mon1 and CCZ-1.

We found that *ccz-1(t2129)* and *ccz-1(ok2182)*, two different mutant alleles of *ccz-1* that lack or have severely reduced activity (Nieto *et al.*, 2010), respectively, similarly resulted in the loss of birefringent gut granules and mislocalization of birefringent material into the intestinal lumen (Figure 2B and Table 2). Consistent with altered gut

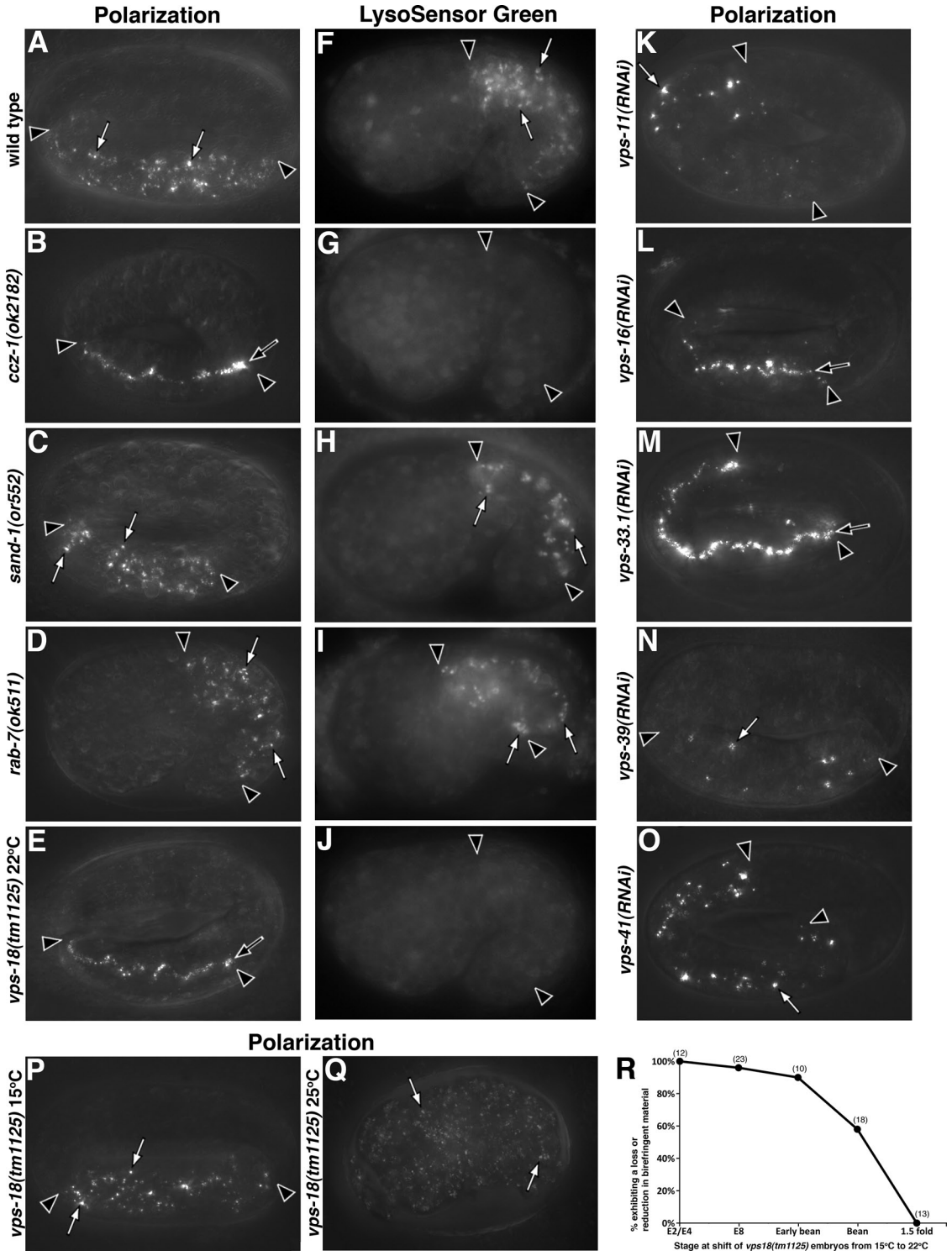

FIGURE 2: Analysis of birefringent and acidified gut granules in embryonic intestinal cells. Embryos were analyzed with polarization microscopy to detect birefringent material, stained with LysoSensor Green, and analyzed with fluorescence microscopy to detect acidified compartments. (A, F) Wild-type, (C, H) *sand-1*, and (D, I) *rab-7* mutant embryos displayed birefringent and acidified gut granules (white arrows). (B, G) *ccz-1* and (E, J) *vps-18* mutants lacked acidified and birefringent gut granules and mislocalized birefringent material into the intestinal lumen (black arrows). (K–O) RNAi targeting subunits of the VPS-C/HOPS complex in an *rrf-3(pk1426)* RNAi–sensitive strain caused a reduction in the number of birefringent organelles (white arrows) and sometimes led to misaccumulation of birefringent material in the intestinal lumen (black arrows). (P, Q) Birefringent material (white arrows) was present within the intestinal cells of *vps-18* mutants at 15°C and was distributed throughout the embryo at 25°C. The intestine is flanked by black arrowheads in A–P. Pretzel-stage embryos are shown in A–C, E, and K–P; 1.5-fold-stage embryos are shown in D and F–J. A terminally arrested pre–bean stage *vps-18* mutant embryo is shown in Q. Embryos are ~50 μm in length. (R) Individual *vps-18* mutant embryos were shifted from 15 to 22°C at the indicated stage, and on reaching threefold stage or later, were

granule formation, *ccz-1* mutant embryos lacked LysoSensor Green–stained compartments (Figure 2G). *ccz-1* mutants also lacked or had substantially reduced numbers of autofluorescent gut granules in adults (Figure 1I and Table 1). The Glo phenotypes exhibited by the *ccz-1(t2129)* mutant were rescued by the introduction of *ccz-1(+)::yfp* (Tables 1 and 2). In contrast to *ccz-1* mutants, the strong loss-of-function *sand-1(or552)* mutant and the likely null *sand-1(ok1963)* mutant (Poteryaev *et al.*, 2007) did not exhibit a loss of birefringent, acidified, or autofluorescent gut granules (Figures 1H and 2, C and H, and Tables 1 and 2), suggesting that SAND-1 does not play a significant role in gut granule biogenesis.

rab-7. *C. elegans* codes for a single RAB-7–related protein, which is orthologous to Rab7 in other organisms (Gallegos *et al.*, 2012). In *C. elegans*, the SAND-1/CCZ-1 complex promotes association of RAB-7 with endosomal membranes (Poteryaev *et al.*, 2007; Kinchen and Ravichandran, 2010; Nieto *et al.*, 2010), likely by acting as a RAB-7 guanine nucleotide exchange factor (GEF; Nordmann *et al.*, 2010; Gerondopoulos *et al.*, 2012). The HOPS complex is an effector of RAB-7 in yeast and possibly other organisms (Nickerson *et al.*, 2009; Epp *et al.*, 2011; Zlatic *et al.*, 2011a). Thus RAB-7 might act as a functional link between CCZ-1 and HOPS during trafficking to gut granules. If this is the case, *rab-7* mutants should exhibit defects in gut granule biogenesis similar to *ccz-1* and VPS-C/HOPS mutants.

The *rab-7(ok511)* null mutant exhibits maternal effect embryonic lethality and arrests at a stage after gut granules are normally formed (Yu *et al.*, 2008), which allowed us to investigate the role of RAB-7 in the biogenesis of gut granules. Whereas the number of autofluorescent gut granules was not substantially reduced in *rab-7* mutants (Figure 1J and Table 1), at the L4 stage their diameter was reduced by 65% relative to wild type (Supplemental Figure S2). The number of birefringent gut granules in *rab-7* mutants was modestly reduced (Table 2); however, unlike *ccz-1* and *vps-18* mutants, birefringent material was never detected in the intestinal lumen (Figure 2D and Table 2). The average diameter of gut granules in 1.5-fold–stage embryos increased from 0.7 µm in wild type to 1.2 µm in *rab-7* mutants (Supplemental Figure S2). Gut granules in *rab-7* mutant embryos were stained by LysoSensor Green (Figure 2I), suggesting that they are acidified. Together these results indicate that loss of *rab-7* function only subtly affects gut granule formation.

Protein trafficking to gut granules

The loss or misaccumulation of gut granule contents might result from specific defects in the formation/trafficking of birefringent or autofluorescent material or more generally from alterations in gut granule biogenesis. In addition, alterations in protein trafficking to gut granules might not obviously affect the localization of these materials.

To address these possibilities, we analyzed the localization of gut granule proteins in the endolysosomal trafficking mutants. CDF-2 and PGP-2 are multipass transmembrane proteins, which at steady state exclusively localize to the gut granule (Figure 3, A and B; Davis *et al.*, 2009; Hermann *et al.*, 2012). The single-pass membrane-associated protein LMP-1 localizes to both gut granules and conventional lysosomes (Hermann *et al.*, 2012). LMP-1 transport to gut granules depends on the activity of the AP-3 adaptor complex, whereas CDF-2::green fluorescent protein (GFP) and PGP-2 can be trafficked to gut granules independently of AP-3 (Hermann *et al.*, 2012). We carried out trafficking studies in 1.5-fold embryos, a stage when both gut granules and these proteins are initially being synthesized within the 20 newly polarized intestinal epithelial cells (Hermann *et al.*, 2005).

Similar to their effects on the localization of birefringent and autofluorescent material, the colocalization of CDF-2::GFP and PGP-2 at gut granules was not disrupted in *sand-1* and *rab-7* mutants (Figure 3, J–P). *sand-1* mutants did not substantially reduce the localization of LMP-1 to gut granules containing CDF-2::GFP and PGP-2 (Figures 4, J–L, and 5, J–L). In contrast, in *rab-7* mutant embryos, LMP-1 levels were significantly reduced and many CDF-2::GFP and PGP-2 compartments lacked detectable LMP-1 (Figures 4, M–P, and 5, M–P). These data indicate that gut granules are formed in *sand-1* and *rab-7* mutants. However, RAB-7 activity promotes the normal accumulation of LMP-1 at the gut granule.

Indicative of a significant defect in gut granule biogenesis, the distribution and colocalization of gut granule proteins were dramatically altered by mutations in *vps-18* and *ccz-1*. PGP-2 and CDF-2::GFP colocalized at gut granules in wild-type 1.5-fold-stage embryos (Figure 3, A–C and P). In *vps-18* mutants, CDF-2::GFP was enriched on organelles that did not contain PGP-2 (Figure 3, D–F and P). In *ccz-1* mutants, CDF-2::GFP was localized to compartments that typically lacked PGP-2, which could be only weakly detected on intestinal organelles (Figure 3, G–I and P). LMP-1, which normally colocalized with PGP-2 on gut granules in wild type (Figure 4, A–C and P), rarely colocalized with PGP-2 in both *vps-18* and *ccz-1* mutants (Figure 4, D–I and P). CDF-2::GFP compartments in wild type contained LMP-1 (Figure 5, A–C and P), whereas a reduced proportion of CDF-2::GFP compartments contained LMP-1 in *vps-18* and *ccz-1* mutants (Figure 5, D–I and P).

Our results indicate that one or more gut granule–associated proteins are mislocalized in embryos deficient for VPS-18 or CCZ-1 function. PGP-2 exhibited weak staining in *vps-18* and *ccz-1* mutants, and LMP-1 normally associates with both gut granules and lysosomes. We therefore examined the localization of CDF-2::GFP in strains with altered VPS-18 and CCZ-1 activity. In *vps-18* mutant embryos, CDF-2::GFP was often associated with organelles located near the apical surface of intestinal cells (compare Figure 6, A and D), which is where conventional lysosomes and early endosomes are typically localized (Hermann *et al.*, 2012). In contrast, CDF-2::GFP–containing compartments were distributed throughout the cytoplasm of *ccz-1* mutants (Figure 3G). In wild-type and both mutant strains, CDF-2::GFP did not accumulate on RAB-5–marked early endosomes (Supplemental Figure S3). Of note, CDF-2::GFP–containing organelles in *vps-18* mutants were often marked by RAB-7, unlike *ccz-1* mutants and wild type (Figure 6, A–I and S). RAB-7 was often associated with endolysosomes marked by LMP-1::GFP (Figure 7, F–H, and Supplemental Figure S2). Consistent with CDF-2::GFP being mislocalized to lysosomes in *vps-18*

analyzed using polarization microscopy. Embryos exhibiting <20 birefringent granules were scored as having a reduced number of granules. E^2, E^4, and E^8 refer to the number of intestinal cells in the intestinal primordium; early-bean-stage embryos are E^{16} before the apical migration of intestinal nuclei. Bean and 1.5-fold stages refer to the body morphology. The number of embryos scored is indicated in parentheses near each data point. Unshifted *vps-18* mutants grown at 15°C exhibited a Glo phenotype only 9% of the time ($n = 33$). Wild-type embryos that underwent similar temperature shifts always displayed >50 birefringent granules.

Genotype	Percentage lacking birefringence in intestinal cells[a]	Percentage with 1–20 birefringent granules in intestinal cells[a]	Percentage with 21–50 birefringent granules in intestinal cells[a]	Percentage with >50 birefringent granules in intestinal cells	*n*
Wild type[b]	0	0	0	100	43
apt-6(ok429)	0	77 (58)	23 (23)	0	31
apt-7(tm920)	0	100 (81)	0	0	27
ccz-1(ok2182)	100 (14)	0	0	0	58
ccz-1(t2129)[c]	100 (38)	0	0	0	90
ccz-1(t2129) + ccz-1::yfp[c]	0	5	71	24	21
glo-3(kx90)	44 (17)	56 (35)	0	0	84
pgp-2(kx48)	0	33	67 (67)	0	21
rab-7(ok511)[d]	0	33	67	0	15
rab-7(RNAi)[e]	2	27	68	2	41
sand-1(ok1963)	0	0	0	100	51
sand-1(or552)	0	0	0	100	49
vps-8(ok2912)[f]	0	0	6	94	32
vps-11(RNAi)[g]	0	92 (28)	8	0	40
vps-16(RNAi)[g]	0	100 (83)	0	0	47
vps-18(tm1125), 15°C	0	6	58	36	33
vps-18(tm1125), 22°C	100 (68)	0	0	0	106
vps-18(tm1125) + vps-18::gfp, 22°C	0	0	0	100	36
vps-33.1(RNAi)[g]	0	82 (38)	18	0	48
vps-33.2(RNAi)[g]	0	0	5	95	37
vps-39 (RNAi)[g]	2	72 (6)	26	0	47
vps-41(RNAi)[g]	0	58 (8)	40	2	40
vps-45(tm246)	0	0	0	100	51
vps-45(RNAi)[g]	0	0	6	94	35
Double mutants				0	
apt-6(ok429); vps-18(tm1125)[h]	85 (66)	15 (11)	0	0	94
apt-7(tm920); vps-18(tm1125)[h]	88 (53)	12 (8)	0	0	74
apt-7(tm920); sand-1(or552)	0	82 (11)	5	3	38
apt-7(tm920); ccz-1(ok2182)	100 (22)	0	0	0	23
apt-6(ok429); rab-7(ok511)[i]	0	83 (35)	17	0	23
apt-7(tm920); rab-7(ok511)[i]	0	96 (44)	8	0	25
glo-3(kx90); rab-7(RNAi)[e]	57 (9)	43 (23)	0	0	131
pgp-2(kx48); rab-7(ok511)[i]	0	100 (20)	0	0	20

All strains were grown at 22°C unless otherwise noted. Threefold- and later-stage embryos were analyzed using polarization microscopy and scored for the presence and localization of birefringent material in the intestine.

[a]Percentage that also mislocalized birefringent material into the intestinal lumen are in parentheses.

[b]The phenotype of wild type was not altered by growth at 15°C (unpublished data).

[c]Dpy progeny of *dpy-11(e224) ccz-1(t2129)/nT1[qIs51]* were isolated, and their progeny were scored. *dpy-11(e224) ccz-1(t2129); jcpEx2[ccz-1::yfp; myo-2::gfp]* embryos expressing GFP were scored. Non–GFP-expressing animals, which lacked *jcpEx2*, were often Glo (not shown).

[d]Non–GFP-expressing *rab-7(-)/rab-7(-)* adults from *rab-7(ok511)/mIn1[mIs14]* parents were isolated, and their embryonic progeny were scored.

[e]RNAi was carried out in an otherwise wild-type background. *F33E2.4(RNAi)* targeting a gene not involved in gut granule formation did not alter the number of birefringent compartments in the indicated strain. All embryos scored displayed numerous enlarged refractile structures visible with DIC microscopy, indicative of *rab-7(-)*.

[f]Non-GFP *vps-8(-)/vps-8(-)* progeny of *vps-8(ok2912)/nT1[qIs51 GFP]* were scored.

[g]RNAi was carried out in the *rrf-3(pk1426)* RNAi–sensitive strain (Simmer *et al.*, 2003). F33E2.4(RNAi) targeting a gene not involved in gut granule formation did not alter number of birefringent compartments in *rrf-3(-)*.

[h]*unc-4(e120)*, which did not alter the Glo phenotype, was present in the background.

[i]Embryonic progeny of *rab-7(-)/rab-7(-); glo(-)/glo(-)* parents were scored.

TABLE 2: Gut granules in embryos.

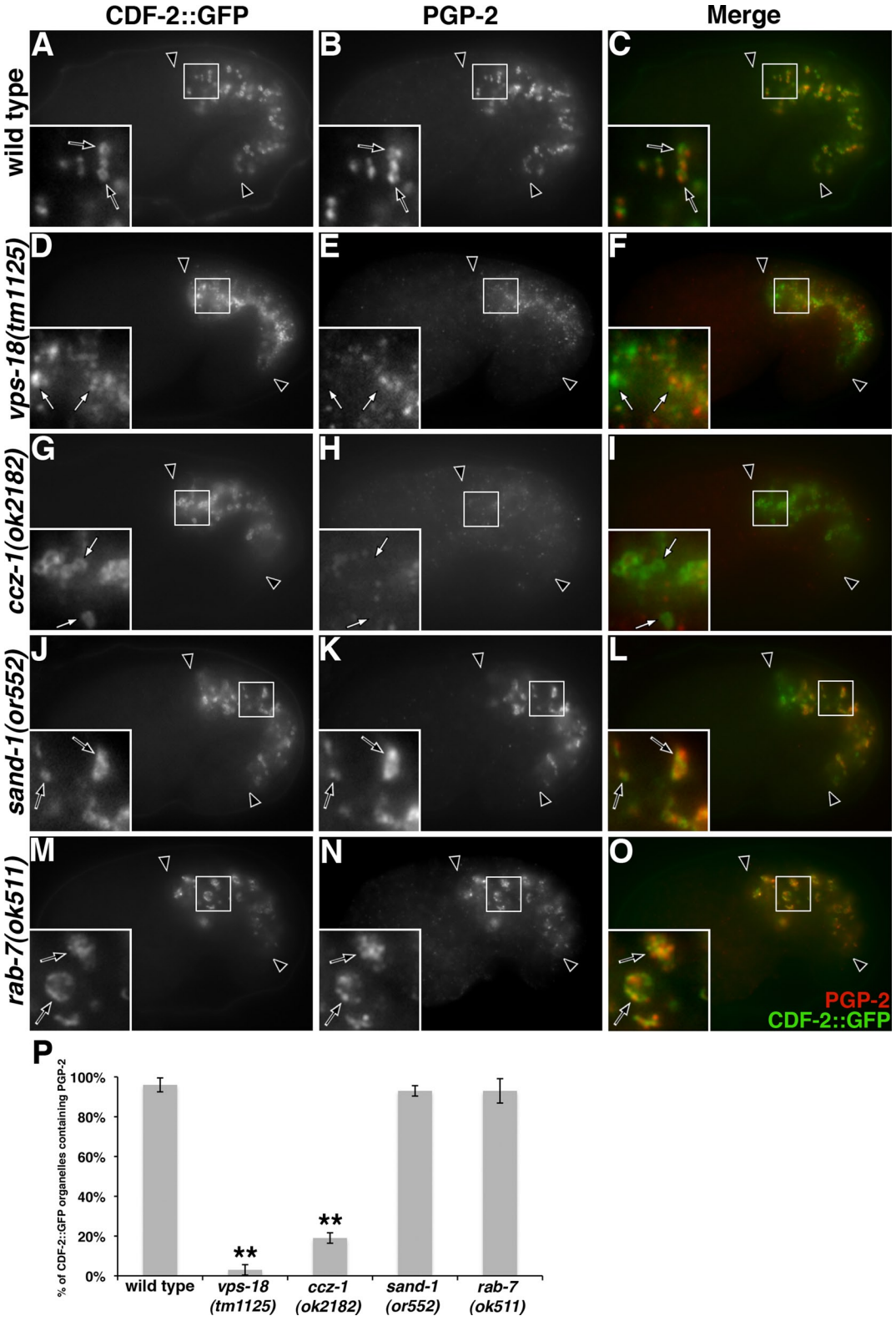

FIGURE 3: The distribution of CDF-2::GFP and PGP-2 is altered in *vps-18* and *ccz-1* mutants. Anti–PGP-2 antibodies and ectopically expressed CDF-2::GFP colocalized at gut granules in (A–C) wild type and (J–L) *sand-1* and (M-O) *rab-7* mutants (black arrows within insets). (D–F) CDF-2::GFP–containing organelles in *vps-18* mutants lacked PGP-2 staining (white arrows in insets). (G–I) The majority of CDF-2::GFP–labeled compartments in *ccz-1* mutants lacked anti–PGP-2 staining (white arrows in insets). In A–O, 1.5-fold-stage embryos are shown, black arrowheads flank the intestine, and the insets are 5 µm wide. (P) For each genotype, at least 25 randomly selected CDF-2::GFP–containing intestinal compartments in five different 1.5-fold-stage embryos were scored for the presence of anti-PGP-2 signals. The mean is plotted, and error bars represent the 95% confidence limit. A one-way analysis of variance (ANOVA) comparing each mutant to wild type was used to calculate *p* values (**$p \leq 0.001$).

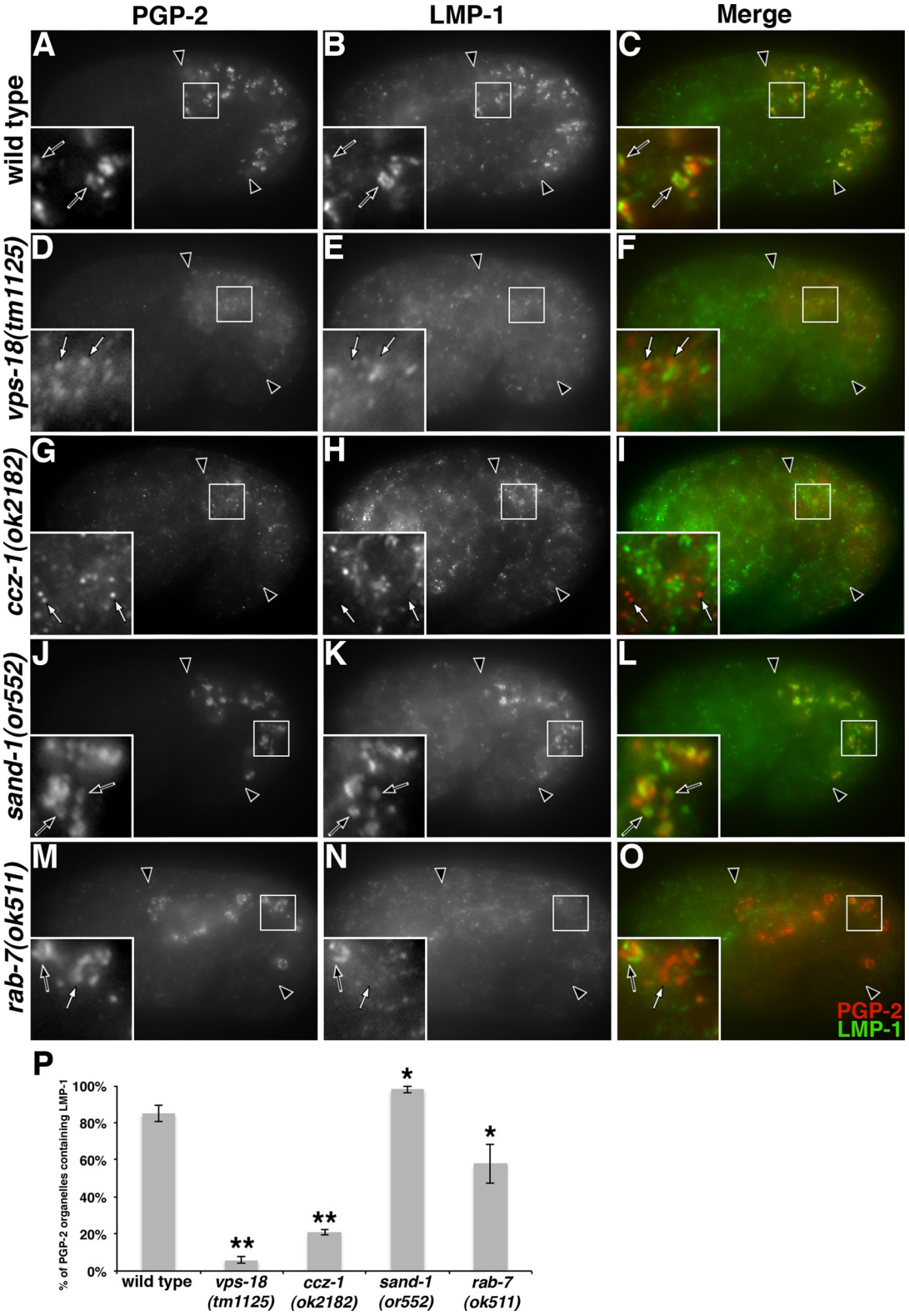

FIGURE 4: The distribution of PGP-2 and LMP-1 is altered in *vps-18*, *ccz-1*, and *rab-7* mutants. Antibodies recognizing PGP-2 and LMP-1 colocalized at gut granules in (A–C) wild type and (J–L) *sand-1* mutants (black arrows in insets). (D–I) PGP-2–stained organelles in *vps-18* and *ccz-1* mutants lacked LMP-1 staining (white arrows within insets). (M–O) In *rab-7* mutants, LMP-1 staining was weakly present on some (black arrows in insets) but not all (white arrows in insets) anti-PGP-2–marked gut granules. In A–O, 1.5-fold-stage embryos are shown, black arrowheads flank the intestine, and insets are 5 μm wide. (P) For each genotype, at least 25 randomly selected PGP-2–stained intestinal compartments in five different 1.5-fold-stage embryos were scored for the presence of LMP-1 staining. The mean is plotted, and error bars represent the 95% confidence limit. A one-way ANOVA comparing each mutant to wild type was used to calculate *p* values (*$p \leq 0.05$, **$p \leq 0.001$).

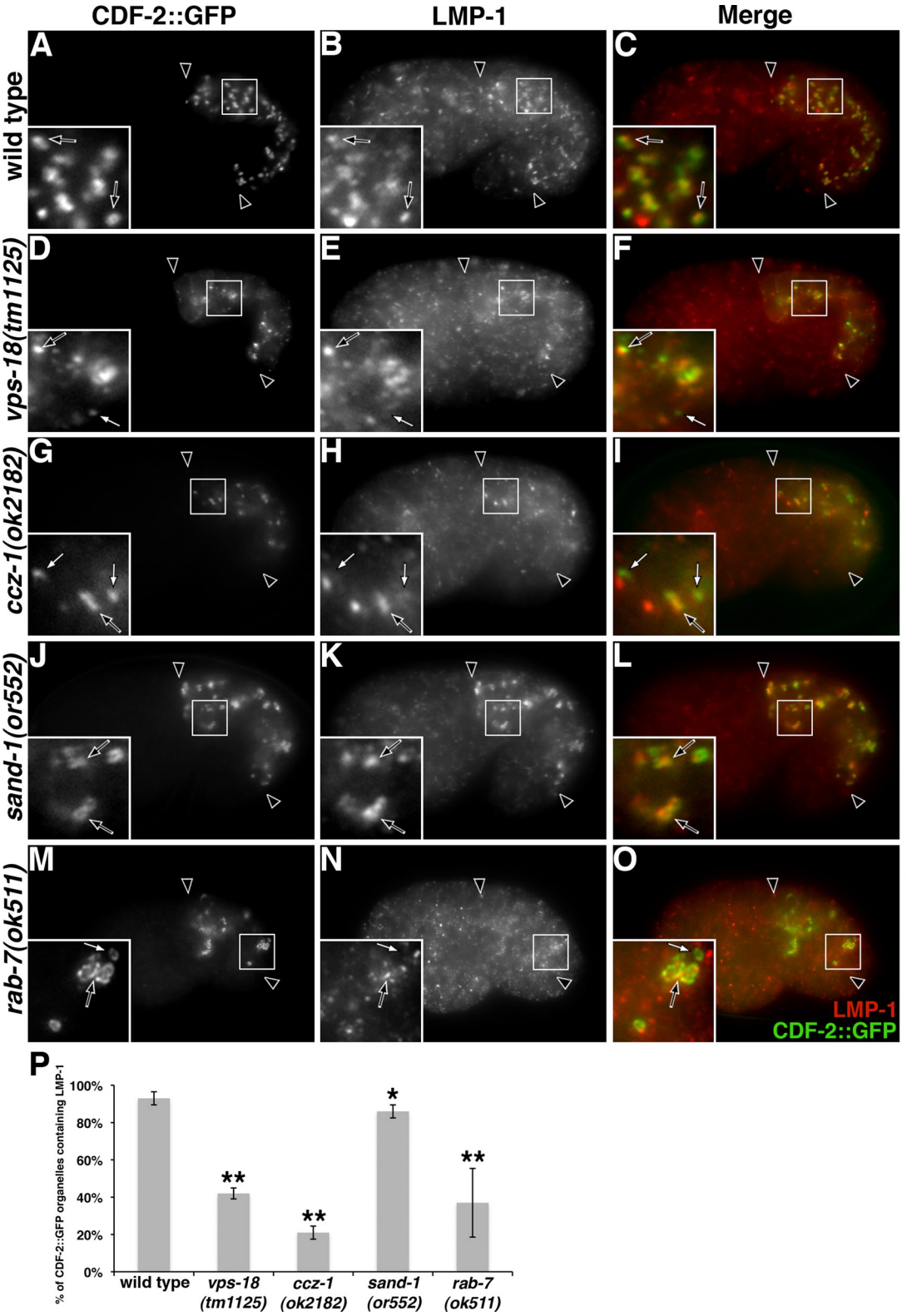

FIGURE 5: The distribution of CDF-2::GFP and LMP-1 is altered in *vps-18*, *ccz-1*, and *rab-7* mutants. Nearly all CDF-2::GFP–containing organelles were marked by anti–LMP-1 antibodies in (A–C) wild-type and (J–L) *sand-1* mutant cells (black arrows in insets). In (D–F) *vps-18*, (G–I) *ccz-1*, and (M–O) *rab-7* mutants, a subset of CDF-2::GFP–marked organelles contained anti–LMP-1 staining (black arrows in insets), although most lacked LMP-1 (white arrows in insets). In A–L, 1.5-fold-stage embryos are shown, and in M–O, a late-bean-stage embryo is shown. In A–O, black arrowheads flank the intestine and insets are 5 μm wide. (P) For each genotype, at least 25 randomly selected CDF-2::GFP–containing intestinal compartments in five different 1.5-fold-stage embryos were scored for the presence of LMP-1 staining. The mean is plotted, and error bars represent the 95% confidence limit. A one-way ANOVA comparing each mutant to wild type was used to calculate *p* values (*$p \leq 0.05$, **$p \leq 0.001$).

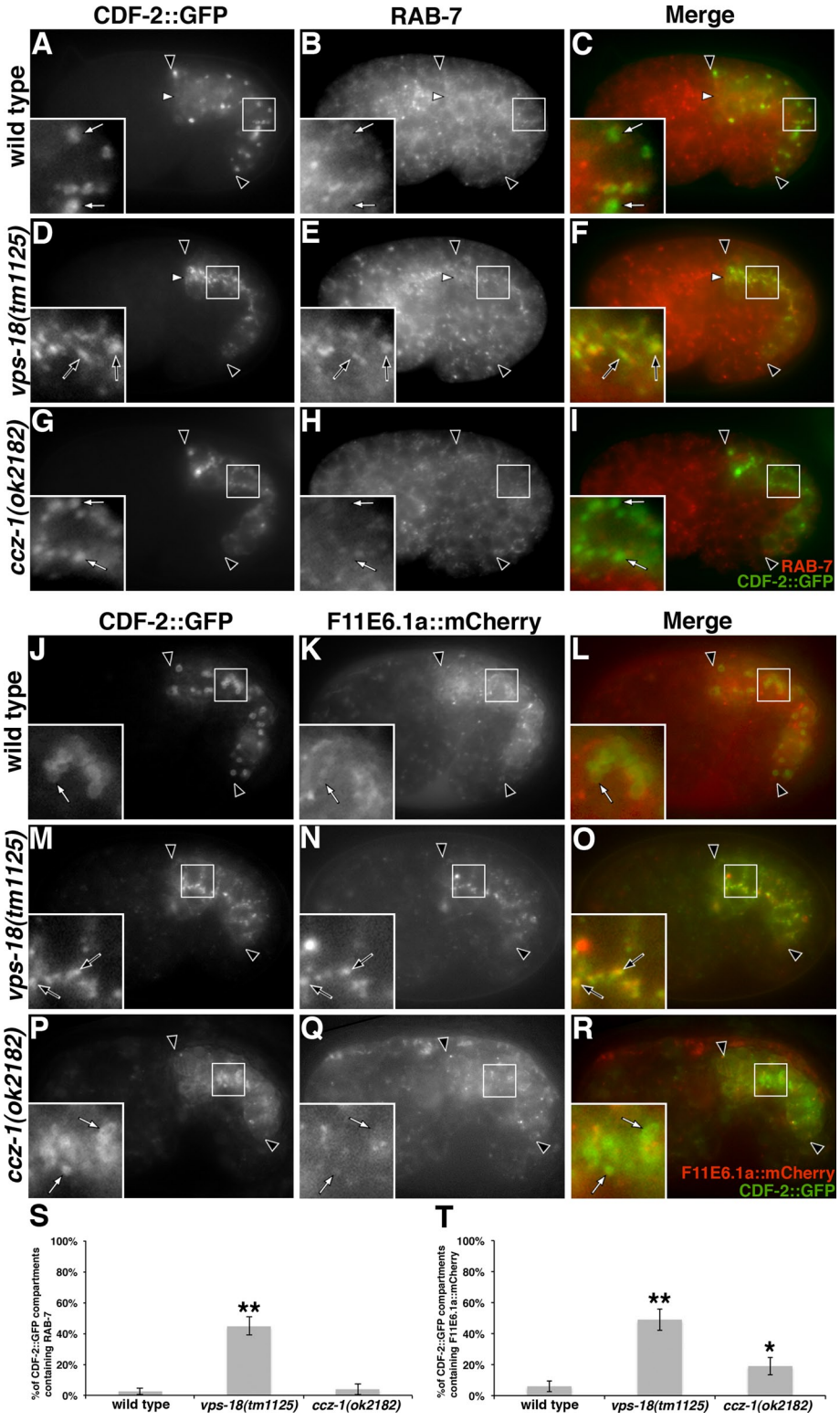

FIGURE 6: CDF-2::GFP is mislocalized to endolysosomes in *vps-18* mutants. (A–C, G–I) Endogenous RAB-7 detected with anti–RAB-7 antibodies was not associated with CDF-2::GFP–containing organelles in wild type or *ccz-1* mutants (white arrows in insets). (D–F) In *vps-18* mutants, anti–RAB-7 staining was often localized to CDF-2::GFP–marked compartments (black arrows in insets). The lysosomal hydrolase F11E6.1a::mCherry did not appreciably localize to CDF-2::GFP–marked compartments in (J–L) wild type or (P–R) *ccz-1* mutants (white arrows in insets). (M–O) In *vps-18* mutants, F11E6.1a::mCherry often colocalized with CDF-2::GFP–containing compartments (black arrows in insets). In A–R, single optical sections of 1.5-fold-stage embryos are shown, black arrowheads flank the intestine, and insets are 5 µm wide. In A–F, white arrowheads denote the apical surface of intestinal cells. (S, T) For each genotype, at least 25 randomly selected CDF-2::GFP–containing intestinal compartments in five different 1.5-fold-stage embryos were scored for the presence of RAB-7 or F11E6.1a::mCherry. The mean is plotted, and error bars represent the 95% confidence limit. A one-way ANOVA comparing each mutant to wild type was used to calculate *p* values (*$p \leq 0.05$, **$p \leq 0.001$).

mutants, CDF-2::GFP colocalized with an mCherry-tagged form of the lysosomal glucosylceramidase F11E6.1a (Levitte *et al.*, 2010; Figure 6, M–O and T). CDF-2::GFP did not appreciably associate with F11E6.1a::mCherry in wild-type or *ccz-1(-)* mutant embryos (Figure 6, P–R and T). The identity of CDF-2::GFP compartments in *ccz-1* mutants is unclear, as they lack markers for gut granules, early endosomes, late endosomes, and lysosomes, whereas disrupting VPS-18 activity results in gut granule proteins being missorted toward conventional lysosomes.

Formation of conventional endolysosomes

In addition to analyzing the effects of the endolysosomal trafficking pathway mutants on gut granule biogenesis, we also examined their role in controlling the number and identity of conventional endolysosomes in the embryonic intestinal primordium. LMP-1::GFP marks conventional lysosomes that are localized near the intestinal cell apical domain of 1.5-fold embryos (Hermann *et al.*, 2012). Wild-type embryos contained on average 12 LMP-1::GFP compartments in the four intestinal cells that make up intestinal rings 2 and 3, whereas *vps-18* mutants displayed fourfold more, which were enriched near the apical cell surface (Figure 7, A, B, and R). Relative to wild type, *ccz-1* mutants had a twofold increase in the number of LMP-1::GFP compartments, which were not restricted to the apical domain (Figure 7, C and R). The number of LMP-1::GFP organelles was only slightly altered in *sand-1* and *rab-7* mutants (Figure 7, D, E, and R).

Owing to effects of *vps-18* and *ccz-1* mutations on the number and localization of LMP-1::GFP–containing compartments, we analyzed the identity of LMP-1::GFP–containing compartments using antibodies to RAB-5 and RAB-7. LMP-1::GFP did not accumulate on RAB-5 marked early endosomes in wild type or in *vps-18* and *ccz-1* mutants (Supplemental Figure S3, J–R and T). Of note, unlike wild type, *vps-18* mutant embryos displayed an increase in the proportion of LMP-1::GFP compartments that also contained RAB-7 (Figure 7, F–K and S),

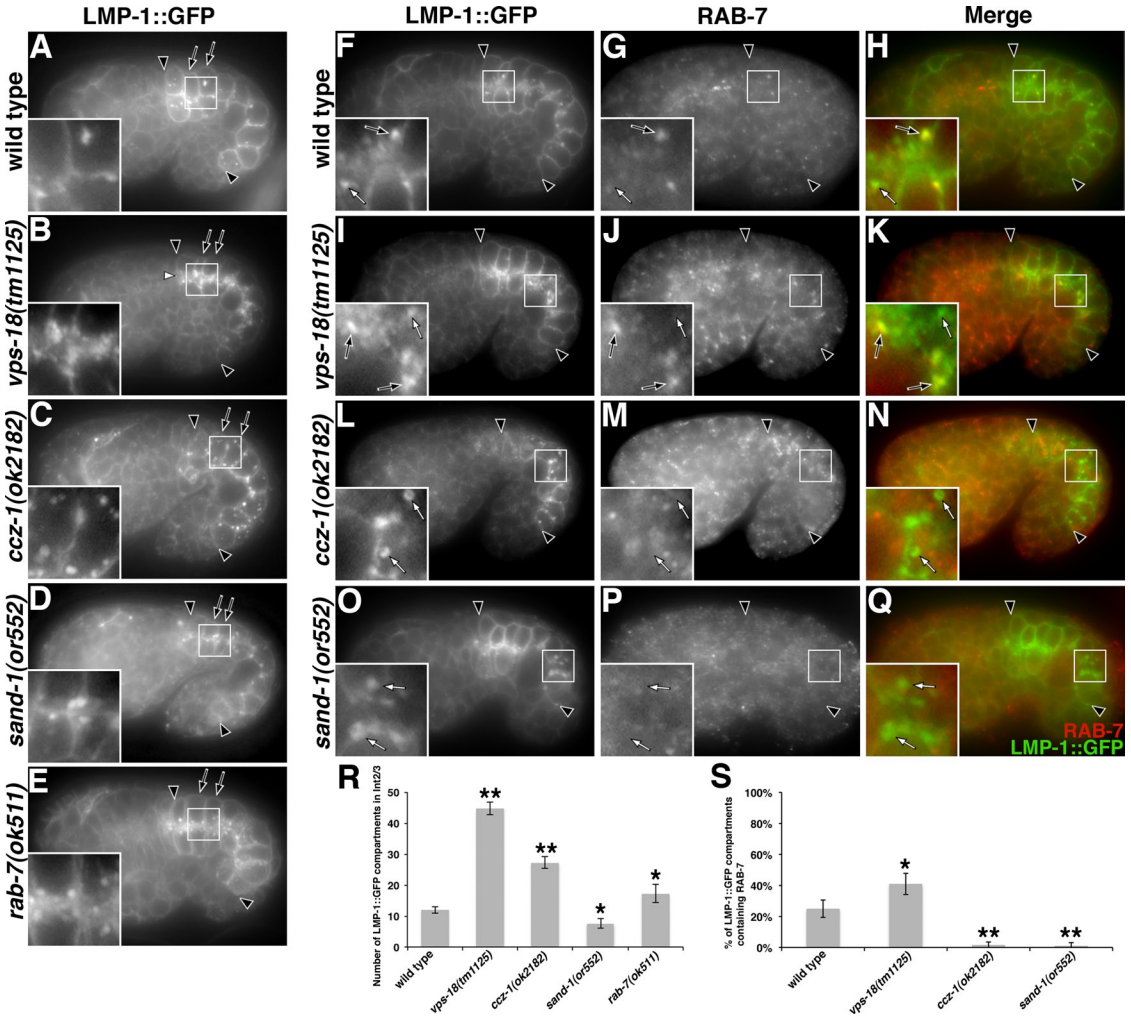

FIGURE 7: Analysis of LMP-1::GFP trafficking. (A–E) Mutations in (B) *vps-18*, (C) *ccz-1*, and to a lesser extent (E) *rab-7* led to an increased number of LMP-1::GFP–marked organelles. (R) The total number of LMP-1::GFP compartments was quantified in the four cells that compose Int2 and Int3 (marked by black arrows in A–E) in five different 1.5-fold-stage embryos of each genotype. The mean is plotted, and error bars represent the 95% confidence limit. A one-way ANOVA comparing each mutant to wild type was used to calculate *p* values (*$p \leq 0.05$, **$p \leq 0.001$). (F–H) Relative to wild type, a higher proportion of LMP-1::GFP compartments in (I–K) *vps-18* mutants contained RAB-7 antibody signals, and a decreased proportion of LMP-1::GFP compartments in (L–N) *ccz-1* and *sand-1* mutants contained RAB-7 (in the insets, black arrows denote LMP-1::GFP compartments marked by RAB-7 antibodies and white arrows label compartments lacking a RAB-7 signal). (S) For each genotype, at least 25 randomly selected LMP-1::GFP–containing intestinal compartments in five different 1.5-fold-stage embryos were scored for the presence of signal from the RAB-7 antibody. The mean is plotted, and error bars represent the 95% confidence limit. A one-way ANOVA comparing each mutant to wild type was used to calculate *p* (*$p \leq 0.05$, **$p \leq 0.001$). In A–E, 1-µm maximum-intensity projections, and in F–Q, single optical sections, of 1.5-fold-stage embryos are shown. The white arrowhead in B denotes the apical cell membrane. In images showing embryos, the black arrowheads flank the intestine. The insets are 5 µm wide.

suggesting that loss of VPS-18 function leads to an excess of late endosomes or lysosomes, consistent with known roles of HOPS promoting heterotypic fusion of late endosomes with lysosomes and homotypic fusion of lysosomes (Nickerson *et al.*, 2009; Balderhaar and Ungermann, 2013; Solinger and Spang, 2013). In contrast, LMP-1::GFP organelles in *ccz-1* and *sand-1* mutants did not contain RAB-7 (Figure 7, L–Q and S), supporting prior observations that CCZ-1 and SAND-1/Mon1 act in conventional lysosome biogenesis by promoting the association of RAB-7 with endolysosomal membranes (Poteryaev *et al.*, 2007; Kinchen and Ravichandran, 2010; Nieto *et al.*, 2010). Our observations also suggest that LMP-1::GFP trafficking is more sensitive to the loss of CCZ-1 than SAND-1 or alternatively that defects in gut granule biogenesis in *ccz-1* mutants, which are not present in *sand-1* mutants, exacerbate effects on LMP-1::GFP localization, leading to the dramatic difference in LMP-1::GFP compartment number and subcellular localization in these two mutants

Interactions between AP-3 and endolysosomal trafficking factors in gut granule biogenesis

The HOPS complex in yeast mediates the docking of AP-3–containing vesicles at the lysosome-like vacuole through direct interactions of AP-3 and a short region of VPS41, which is conserved in *C. elegans* VPS-41 (Angers and Merz, 2009; Cabrera *et al.*, 2010).

In mammalian cells, HOPS subunits colocalize and physically interact with AP-3 subunits (Zlatic *et al.*, 2011b). The AP-3 adaptor complex has evolutionarily conserved roles in trafficking to LROs (Dell'Angelica, 2009); however, the functional relationship between AP-3 and HOPS in the biogenesis of LROs has not been investigated.

If VPS-C/HOPS activity is restricted to the same step as AP-3 during trafficking to gut granules, then AP-3 and VPS-C/HOPS mutants should have similar defects in gut granule biogenesis, and the mutants should not exacerbate each other's phenotypes. Inconsistent with this model, *vps-18* mutant embryos completely lacked birefringent intestinal granules, whereas they were always present in null mutants of *apt-6* and *apt-7*, which encode AP-3 β- and μ-subunits, respectively (Table 2). Moreover, the majority of AP-3; *vps-18* double-mutant embryos exhibited a complete loss of birefringent gut granules, resembling the *vps-18* mutant (Table 2). Single VPS-C/HOPS and AP-3 mutants similarly displayed reduced numbers of autofluorescent gut granules (Table 1). However, the *vps-18* mutation, which did not exhibit decreased numbers of autofluorescent compartments on its own at 22°C, led to a complete loss of autofluorescent gut granules when introduced into both *apt-6* and *apt-7* mutant backgrounds (Table 1). A *vps-41* mutation also enhanced the adult Glo phenotype of the *apt-6* mutant (Table 1). Together these genetic interactions suggest that VPS-C/HOPS and AP-3 function at distinct steps in the biogenesis of gut granules.

We also examined whether CCZ-1 has functions distinct from AP-3 in trafficking to gut granules. The application of *ccz-1(RNAi)*, which led to a moderate decrease in the number of autofluorescent gut granules on its own, significantly enhanced the Glo phenotype of *apt-6* and *apt-7* mutants (Table 1). Similarly, autofluorescent and birefringent compartments, which were always present in AP-3 mutants, were absent in an *apt-7; ccz-1* double mutant (Tables 1 and 2). These results point to CCZ-1 having activities that are distinct from those of AP-3.

We extended our analyses of the interactions between mutations disrupting the function of AP-3, VPS-C/HOPS, and CCZ-1 by comparing their effects, alone or in combination, on the relative localization of two gut granule proteins, CDF-2::GFP and PGP-2. Whereas *vps-18* mutants rarely displayed CDF-2::GFP compartments containing PGP-2 (Figures 3, D–F, and 8J), ~25% of CDF-2::GFP compartments were marked by PGP-2 in *apt-7* and *ccz-1* single mutants (Figures 3, G–I, and 8, A–C and J). We found that CDF-2::GFP compartments were more likely to contain PGP-2 in *apt-7; vps-18* and *apt-7; ccz-1* double mutants than the single mutants (Figure 8, D–J). The ability of an AP-3 mutant to modify the effects of mutations in *vps-18* or *ccz-1* on the colocalization of CDF-2::GFP and PGP-2 suggests that AP-3 functions upstream of, or parallel to, VPS-C/HOPS and CCZ-1 in trafficking to the gut granule.

We used AP-3 and other *glo* mutants that exhibit partial defects in gut granule biogenesis and are thus sensitized to reveal gene function in the pathway to investigate whether SAND-1/Mon1 and RAB-7 play roles in trafficking to gut granules not apparent in an otherwise wild-type background. We found that mutations in *sand-1* did not alter the Glo phenotype of *apt-7* mutant embryos or adults (Tables 1 and 2). Moreover, the codistribution of gut granule proteins was not significantly different between *apt-7* single and *apt-7; sand-1* double mutants (Supplemental Figure S4). Thus we find no evidence supporting a role for SAND-1 in gut granule formation. The number of autofluorescent gut granules in AP-3*; rab-7* mutant embryos and adults was not obviously different from that in AP-3 mutants (Tables 1 and 2). Similarly, the few autofluorescent gut granules in *glo-2* mutant adults and birefringent gut granules in *glo-3* mutant embryos remained in double mutants with *rab-7* (Tables 1 and 2). However, the introduction the *rab-7* mutation weakly enhanced the Glo phenotypes of *pgp-2* mutant adults and embryos and *glo-3* mutant adults. Similar to our analysis of protein trafficking, our genetic studies point to RAB-7 selectively and subtly contributing to gut granule formation.

GLO-1(ΔG4) mutants suppress *ccz-1(-)* and *glo-3(-)*

Our work shows that CCZ-1 and VPS-C/HOPS promote gut granule formation. In the lysosome biogenesis pathway, CCZ-1 likely functions with SAND-1/Mon1 as a GEF to activate RAB-7, which, through its effector HOPS, mediates protein trafficking by promoting membrane tethering and fusion (Nickerson *et al.*, 2009; Zlatic *et al.*, 2011a; Balderhaar and Ungermann, 2013). We show that *rab-7* mutants do not phenocopy *ccz-1* mutants, suggesting the possibility that a different Rab protein functions downstream of CCZ-1 in trafficking to the gut granule. Recently HPS-4, one of two mammalian homologues of CCZ-1, was identified as a subunit of the GEF that activates Rab32 and Rab38 (Gerondopoulos *et al.*, 2012). GLO-1, which is known to function in gut granule formation, is the *C. elegans* Rab GTPase most homologous to these proteins (Hermann *et al.*, 2005).

We used an in vivo genetic approach to analyze whether CCZ-1 might function as an upstream activator of the GLO-1 Rab to promote gut granule formation. If CCZ-1 acts as a GEF to activate GLO-1 in the gut granule biogenesis pathway, then it is possible that *ccz-1* mutants are Glo due to the GLO-1 Rab being in its inactive GDP-bound form. To examine this possibility, we generated three different point mutations in the G4 domain of GLO-1 that are predicted to weaken the molecular interactions between GLO-1 and guanine nucleotides (Figure 9S). Analogous mutations in Rab7, which is in the same Rab subfamily as GLO-1 (Klopper *et al.*, 2012; Rojas *et al.*, 2012), led to greatly increased rates of spontaneous guanine nucleotide exchange in vitro and the ability to bypass the necessity of its corresponding GEF in vivo (Kucharczyk *et al.*, 2001; McCray *et al.*, 2010; Nordmann *et al.*, 2010; Cabrera and Ungermann, 2013). We collectively refer to the GLO-1(K130E), GLO-1(D132A), and GLO-1(I133F) mutations as GLO-1(ΔG4) (Figure 9S). The mutations were created in a rescuing GFP-tagged form of GLO-1 (Hermann *et al.*, 2005), which was expressed under the control of the *vha-6* intestinal cell–specific promoter (Oka *et al.*, 2001; Pujol *et al.*, 2001). When introduced into a *glo-1(zu437)* null mutant background (Hermann *et al.*, 2005), two of the point mutants exhibited rescuing activity similar to wild-type GLO-1, whereas GLO-1(K130E) was partially active (Table 3). None of the GLO-1(ΔG4) mutants exhibited dominant Glo phenotypes when expressed in wild type (unpublished data). The majority of *ccz-1* mutant young adults expressing GFP::GLO-1 exhibited a low number of autofluorescent compartments, similar to *ccz-1* mutants alone (Figure 9, B and C, and Table 3). In contrast, expression of all of the GLO-1(ΔG4) mutants significantly increased the number of autofluorescent organelles in *ccz-1* mutants, with the majority of GLO-1(D132A)–containing animals resembling wild type (Figure 9, D and E, and Table 3). Consistent with the compartments being gut granules, the GLO-1(D132A) and GLO-1(I133F) constructs, which exhibited the strongest suppression, restored acidified organelles in *ccz-1* mutants (Figure 9, K–N). These results are consistent with CCZ-1 acting upstream of, or parallel to, the GLO-1 Rab to promote gut granule biogenesis.

We examined the specificity of the genetic interactions between the GLO-1(ΔG4) and *ccz-1* mutants by testing whether the GLO-1(ΔG4) constructs altered the Glo phenotype of other mutants that disrupt gut granule biogenesis. It has been suggested that GLO-4

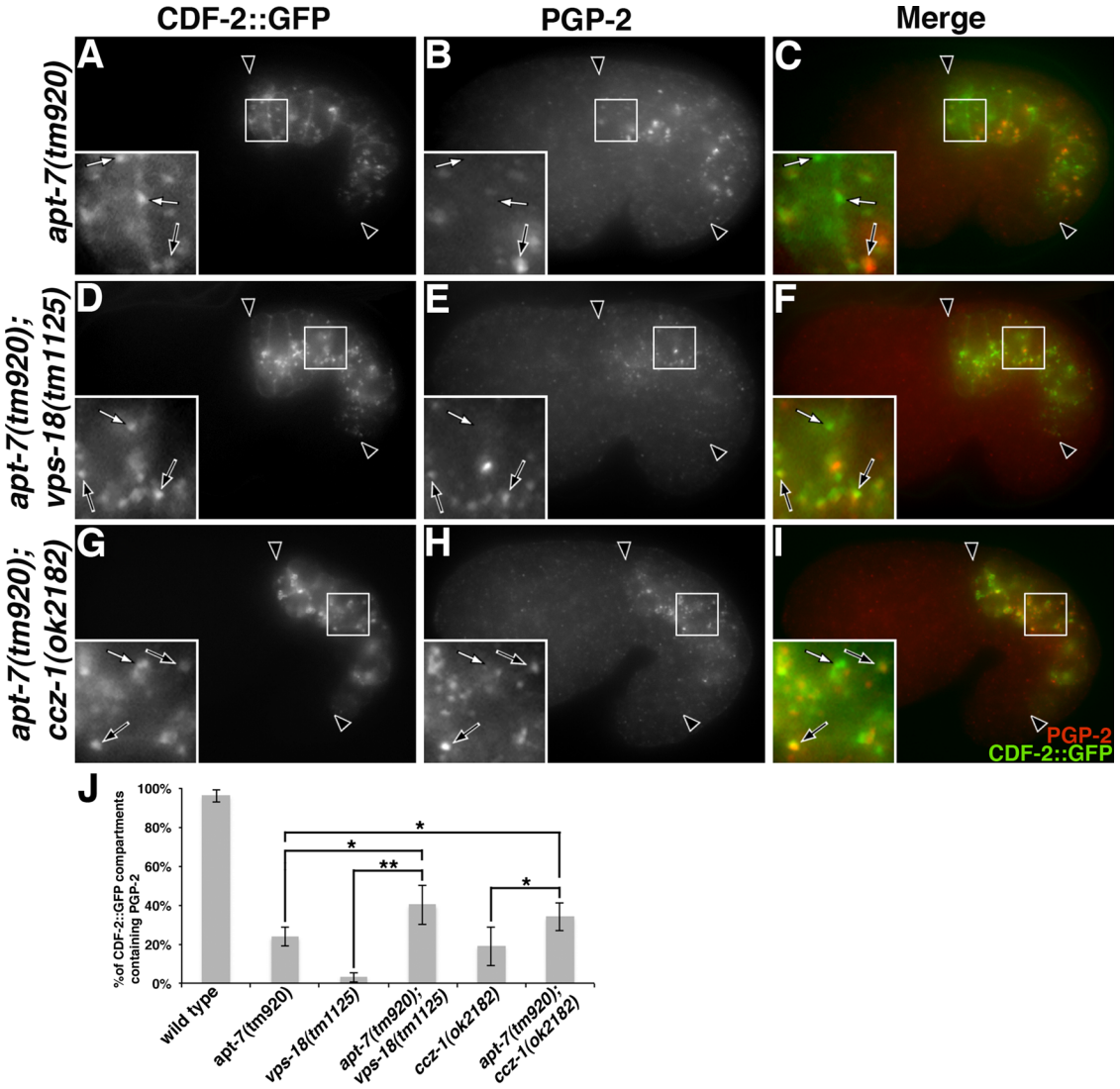

FIGURE 8: Effects of disrupting *vps-18* and *ccz-1* function on gut granule protein trafficking in *apt-7* mutants. Embryos expressing CDF-2::GFP were stained with anti–PGP-2 antibodies. (A–C) In *apt-7* single mutants, CDF-2::GFP–labeled compartments were rarely marked by PGP-2 antibodies (white and black arrows in insets). (D–I) Relative to the single mutants, *apt-7; vps-18* and *apt-7; ccz-1* double mutants displayed an increased proportion of organelles that contained both CDF-2::GFP and PGP-2 (black arrows in insets). (J) For each genotype, at least 25 randomly selected CDF-2::GFP–containing intestinal compartments in five different 1.5-fold-stage embryos were scored for the presence of PGP-2 staining. The mean is plotted, and error bars represent the 95% confidence limit. A one-way ANOVA comparing the indicated genotypes was used to calculate *p* values (*$p \leq 0.05$, **$p \leq 0.001$). In A–I, 1.5-fold-stage embryos are shown, and black arrowheads flank the intestine. The insets are 5 µm wide.

and its homologues act as a GEF for Rabs similar to GLO-1 (Ma *et al.*, 2004; Hermann *et al.*, 2005). However, the GLO-1(ΔG4) mutants did not suppress the Glo phenotype displayed by *glo-4* mutants (Table 3). Similarly, *apt-6* mutants were not rescued by introduction of GLO-1(ΔG4) constructs (Table 3), suggesting that the GLO-1(ΔG4) mutants do not generally restore gut granules in mutants with a partial Glo phenotype similar to *ccz-1*. Finally, we tested the ability of GLO-1(ΔG4) mutants to bypass the activity of BLOC-1, a complex that has evolutionarily conserved roles in LRO biogenesis, and found that the Glo phenotype resulting from mutations in two BLOC-1–encoding subunit genes, *glo-2* and *snpn-1*, were not suppressed by GLO-1(ΔG4) constructs (Table 3).

CCZ-1 and its homologues are believed to function in a heterodimeric complex with a SAND-1/Mon1–related protein (Levine *et al.*, 2013). Our results indicate that SAND-1 does not act with CCZ-1 to promote gut granule biogenesis. To identify other *C. elegans* genes that could function with CCZ-1, we performed PSI-BLAST searches with SAND-1/HPS1 family members from other species. Starting with *Drosophila* HPS1 (Lee *et al.*, 2009), the fourth PSI-BLAST iteration led to the identification of *C. elegans* GLO-3, which shows low but significant similarity to human and *Drosophila* HPS1 proteins (Figure 9T). The region of highest homology with SAND-1/HPS1 family members contains a Longin domain (Kinch and Grishin, 2006), which consists of five β-strands sandwiched between α-helices (Filippini *et al.*, 2001; Tochio *et al.*, 2001). Longin domains are found in a variety of proteins that mediate membrane trafficking and notably are often present in Rab GEFs, where they mediate interactions with Rabs and other Longin

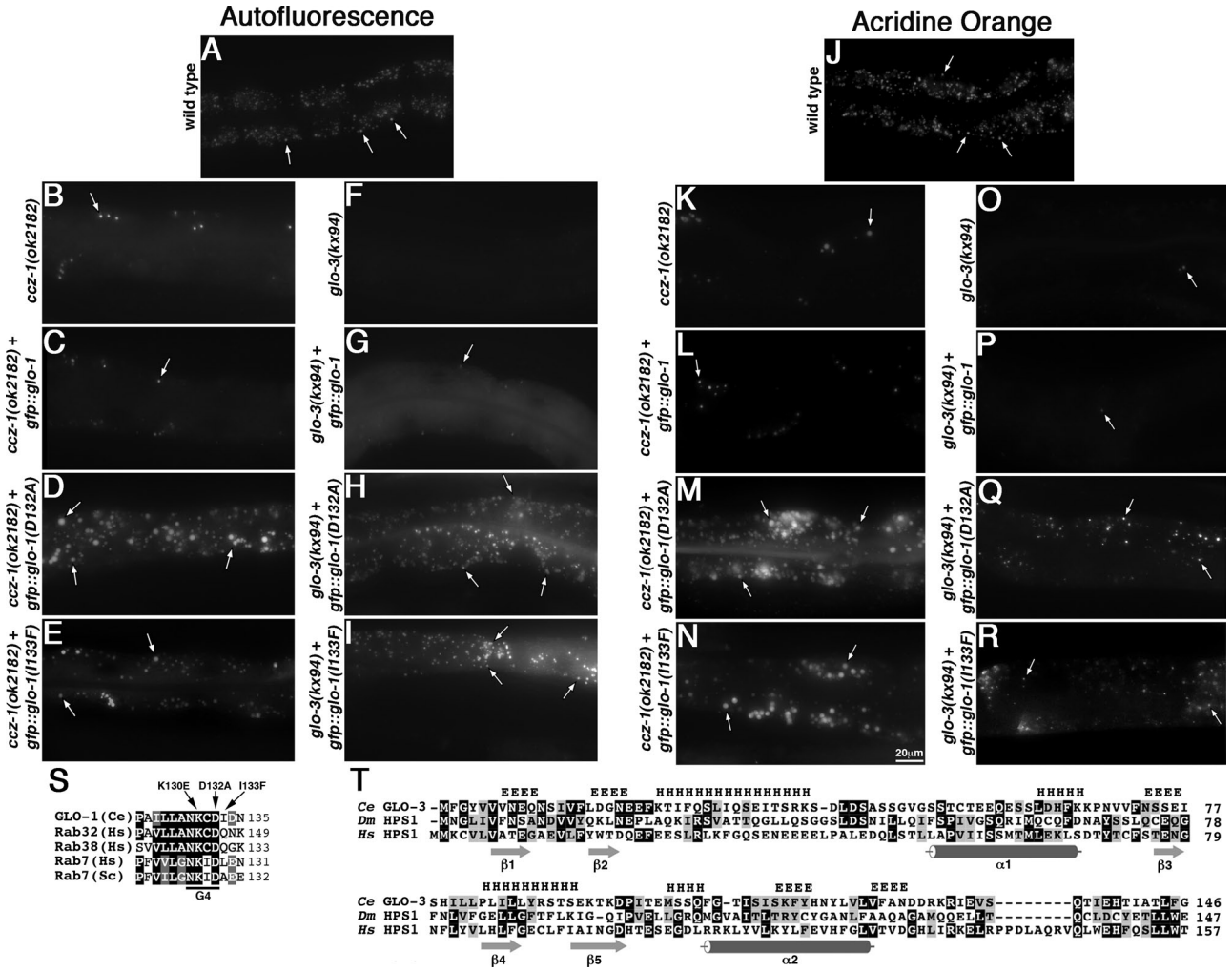

FIGURE 9: Expression of GFP::GLO-1(ΔG4) mutants leads to increased numbers of autofluorescent and acidified gut granules in *ccz-1* and *glo-3* mutants. Young adults were analyzed for the presence of autofluorescent material or the accumulation of the acidophilic dye acridine orange. (A, J) Wild type contained many autofluorescent and acridine orange–stained organelles. (B, C, F, G, K, L, O, and P) *ccz-1* and *glo-3* mutants contained few autofluorescent and acridine orange–stained gut granules, whose numbers did not increase upon the expression of *gfp::glo-1* under control of the *vha-6* promoter. (D, E, H, I, M, N, Q, and R) The addition of *glo-1(D132A)* or *glo-1(I133F)*, which contain mutations in the G4 motif of GLO-1, led to increased numbers of autofluorescent and acridine orange–labeled compartments in *ccz-1* and *glo-3* mutants. Maximum-intensity projections of fluorescence signals spanning the entire depth of the anterior intestine are shown. White arrows denote autofluorescent or acridine orange–stained organelles. (S) Alignment of the G4 domain of *C. elegans* (Ce) GLO-1 and related Rab proteins from humans (Hs) and yeast (Sc), denoting the location of mutations predicted to alter guanine nucleotide binding. (T) Alignment of the amino-terminal region of *C. elegans* GLO-3 (Ce) and HPS-1 from *D. melanogaster* (Dm) and humans (Hs). Location of β-sheets and α-helices that compose the Longing domain in HPS1 proteins are present below the sequences. A consensus of GLO-3 secondary structural predictions for β-sheets (listed as E) and α-helices (listed as H) are positioned above the sequences.

domain–containing proteins (Collins *et al.*, 2002; Kim *et al.*, 2006; Yu *et al.*, 2009; Marat *et al.*, 2011; Levine *et al.*, 2013; De Franceschi *et al.*, 2014). Predictions of GLO-3 secondary structure suggest that GLO-3 has similarity to the first half of the Longin domain (Figure 9T).

glo-3 was identified in a genetic screen for factors that promote gut granule biogenesis, and *glo-3* and *ccz-1* mutants exhibit similar Glo phenotypes (Figure 9F; Rabbitts *et al.*, 2008). We found that expression of two different GLO-1(ΔG4) mutants significantly increased the number of autofluorescent organelles in *glo-3* mutants when compared with expression of wild-type GLO-1 (Figure 9, F–I, and Table 3). The GLO-1(ΔG4) constructs also increased the number of acidified organelles in *glo-3* mutants (Figure 9O-R), suggesting that they lead to restoration of gut granules. These observations suggest that GLO-3 functions similarly to CCZ-1 and are consistent with both proteins acting upstream of the GLO-1 Rab.

DISCUSSION

HOPS function in LRO biogenesis

We showed that all six proteins predicted to compose the canonical HOPS complex in *C. elegans* are necessary for the formation of autofluorescent gut granules (Figure 1 and Tables 1 and 2). This requirement resembles that seen in *Drosophila melanogaster*, where disrupting the HOPS subunits Vps16A (Pulipparacharuvil *et al.*, 2005), *deep orange*/Vps18 (Sevrioukov *et al.*, 1999), *carnation*/Vps33A (Akbar *et al.*, 2009), or *light*/Vps41 (Warner *et al.*, 1998)

Genotype	Percentage of animals with the specified number of autofluorescent granules in anterior intestinal cells						
	0	1–20	21–50	51–100	101–200	>200	*n* (*p* value)
Wild type	0	0	0	0	0	100	83
apt-6(ok429)	50	46	4	0	0	0	52
apt-6(ok429) + gfp::glo-1	60	34	6	0	0	0	32
apt-6(ok429) + gfp::glo-1(D132A)	50	41	9	0	0	0	34
apt-6(ok429) + gfp::glo-1(I133F)	20	73	7	0	0	0	26*
ccz-1(ok2182)[a]	19	67	14	0	0	0	99
ccz-1(ok2182) + gfp::glo-1	6	44	42	8	0	0	53
ccz-1(ok2182) + gfp::glo-1(K130E)	0	17	46	18	12	7	60**
ccz-1(ok2182) + gfp::glo-1(D132A)	0	0	0	0	28	72	25**
ccz-1(ok2182) + gfp::glo-1(I133F)	0	4	32	24	32	8	25**
glo-1(zu437)	100	0	0	0	0	0	35
glo-1(zu437) + gfp::glo-1	0	0	0	0	100	0	52**
glo-1(zu437) + gfp::glo-1(K130E)	0	0	56	44	0	0	72**
glo-1(zu437) + gfp::glo-1(D132A)	0	0	0	0	100	0	71**
glo-1(zu437) + gfp::glo-1(I133F)	0	0	0	0	100	0	68**
glo-2(zu455)	43	55	2	0	0	0	67
glo-2(zu455) + gfp::glo-1	39	51	10	0	0	0	31
glo-2(zu455) + gfp::glo-1(D132A)	32	65	3	0	0	0	34
glo-2(zu455) + gfp::glo-1(I133F)	29	62	7	2	0	0	45
glo-3(kx94)	67	18	5	5	4	1	85
glo-3(kx94) + gfp::glo-1	51	41	8	0	0	0	37
glo-3(kx94) + gfp::glo-1(D132A)	1	0	18	17	24	40	68**
glo-3(kx94) + gfp::glo-1(I133F)	7	32	3	3	13	38	52**
glo-4(ok623)	100	0	0	0	0	0	33
glo-4(ok623) + gfp::glo-1	100	0	0	0	0	0	30
glo-4(ok623) + gfp::glo-1(K130E)	100	0	0	0	0	0	61
glo-4(ok623) + gfp::glo-1(D132A)	100	0	0	0	0	0	64
glo-4(ok623) + gfp::glo-1(I133F)	100	0	0	0	0	0	63
snpn-1(tm1892)	86	14	0	0	0	0	43
snpn-1(tm1892) + gfp::glo-1	60	40	0	0	0	0	35
snpn-1(tm1892) + gfp::glo-1(D132A)	59	41	0	0	0	0	34
snpn-1(tm1892) + gfp::glo-1(I133F)	63	34	3	0	0	0	38

All strains were grown at 22°C unless otherwise noted. Individual young adult-stage animals were analyzed using fluorescence microscopy with a rhodamine filter set and were scored for the number of autofluorescent organelles within the anterior intestine located between the pharynx and vulva. The expression of GLO-1 was verified in all animals scored by the presence of GFP. A Fisher's exact test was used to compare a mutant expressing *gfp::glo-1* to the same mutant expressing a *gfp::glo-1(ΔG4)* variant. $^{**}p \leq 0.001$, $^{*}p \leq 0.05$, lack of asterisk indicates $p > 0.05$.

[a]All *ccz-1(-)* animals scored with or without *gfp::glo-1* transgenes were *ccz-1(-)/ccz-1(-)* progeny of *ccz-1(-)/+* adults. They were identified by containing within their uterus embryos with large refractile bodies visible with DIC microscopy.

TABLE 3: Effects of GLO-1(ΔG4) mutants on gut granule formation.

leads to altered eye pigment, likely from the reduced number of LROs (pigment granules) present within the retinal epithelium (Lloyd *et al.*, 1998). Similarly, in zebrafish, mutations in *platinum/vps11* (Thomas *et al.*, 2011), *vps18* (Sadler *et al.*, 2005; Maldonado *et al.*, 2006), and *lbk/vps39* (Schonthaler *et al.*, 2008) disrupt LRO biogenesis, reducing the number of epidermal and retinal melanosomes. Only one HOPS subunit, Vps33a, has been shown to facilitate the formation of LROs in mammals; the *buff/Vps33a* partial-loss-of-function mutant exhibits reduced numbers of melanosomes and platelet dense granules in mice (Suzuki *et al.*, 2002; Nguyen and Wei, 2004), both characteristics of HPS (Huizing *et al.*, 2008). Mutations in HOPS subunit encoding genes have not been detected in HPS patients, likely due to their essential roles during mammalian embryogenesis (Messler *et al.*, 2011; Aoyama *et al.*, 2012; Peng *et al.*, 2012).

Paralogues of VPS16 and VPS33 do not appear to function during *C. elegans* gut granule formation (Tables 1 and 2) or pigment

granule biogenesis in other organisms (Matthews *et al.*, 2005; Akbar *et al.*, 2009). Instead, they act in the formation of different LROs, epidermal lamellar bodies, and platelet α-granules in mammals (Lo *et al.*, 2005; Hershkovitz *et al.*, 2008; Urban *et al.*, 2012) and fibrous body-membranous organelles in *C. elegans* spermatocytes (Zhu and L'Hernault, 2003; Zhu *et al.*, 2009). It is possible that the canonical HOPS complex (containing VPS11, VPS16a, VPS18, VPS33a, VPS39, VPS41) and an alternate HOPS-related complex (substituting Vps16b for Vps16a and Vps33b for Vps33a) function in the biogenesis of different types of LROs.

Unlike other HOPS-complex mutants in *C. elegans*, which are maternal effect lethal, the conditional *vps-18(tm1125)* mutant provided us with the opportunity to assess the function of VPS-18 during endolysosome and LRO biogenesis in the developing intestinal primordium. We found that loss of *vps-18* activity resulted in a dramatic increase in LMP-1::GFP–containing conventional endolysosomes (Figure 7), similar to what was seen in coelomocytes of *vps-18* mutants (Xiao *et al.*, 2009). *Drosophila* epithelial cells lacking *vps16A* or *vps33A* activity also display increased number of endolysosomes (Pulipparacharuvil *et al.*, 2005; Akbar *et al.*, 2009), and compromising *vps39* or *vps41* activity in cultured mammalian cells leads to more late endosomes due to their impaired fusion with lysosomes (Pols *et al.*, 2013). Disrupting HOPS-subunit function in *C. elegans* phagocytes leads to the accumulation of undegraded phagosomes, likely due to defects in the fusion of lysosomes with RAB-7–containing phagosomes (Kinchen *et al.*, 2008; Xiao *et al.*, 2009). Our data show that LMP-1::GFP compartments in *vps-18* mutants more often contained RAB-7 than did those in wild type (Figure 7). This suggests that in the intestinal primordium, VPS-18 promotes the fusion of lysosomes with late endosomes, a well-documented function of the HOPS complex (Epp *et al.*, 2011; Balderhaar and Ungermann, 2013; Solinger and Spang, 2013). Based on these phenotypes, it is likely that VPS-18 acts as part of the HOPS complex to direct the dynamics of late endosomal and lysosomal membranes in the embryonic intestine.

Our work strongly suggests that VPS-18 mediates gut granule formation due to its activity as a HOPS subunit. Analysis of five distinct gut granule markers indicates that *vps*-18 mutant embryos completely lack gut granules (Figures 2–5). The reduction in the number of autofluorescent and birefringent gut granules and misaccumulation of birefringent material by mutations or RNAi targeting all of the other HOPS-subunit-encoding genes (Figures 1 and 2 and Tables 1 and 2), including the HOPS-specific genes *vps-39* and *vps-41*, point toward HOPS acting in the biogenesis of gut granules. Furthermore, loss of VPS-18 is predicted to lead to the disassembly of the HOPS complex (Plemel *et al.*, 2011). The only known HOPS-independent function of VPS18 is as a subunit in the related CORVET complex (Nickerson *et al.*, 2009; Balderhaar and Ungermann, 2013; Solinger and Spang, 2013). We did not detect an alteration in gut granule biogenesis when *vps-8* activity was disrupted (Tables 1 and 2), which is predicted to specifically disrupt CORVET activity.

The HOPS and AP-3 complexes have evolutionarily conserved roles in protein trafficking to LROs, and their functional interactions are poorly understood (Dell'Angelica, 2009; Zlatic *et al.*, 2011a). In *Saccharomyces cerevisiae*, which lacks LROs, HOPS mediates the tethering and consumption of Golgi-derived, AP-3–containing vesicles by promoting their fusion with conventional lysosomes (Darsow *et al.*, 2001; Angers and Merz, 2009). This process is mediated by direct physical interactions between VPS41, associated with HOPS on the lysosomal membrane, and subunits of the AP-3 vesicle coat (Darsow *et al.*, 2001; Angers and Merz, 2009; Cabrera *et al.*, 2010). Our double-mutant analysis leaves open the possibility that HOPS functions downstream of AP-3, possibly in the same pathway, during trafficking to gut granules (Table 2 and Figure 8).

Our genetic studies also indicate that HOPS function in gut granule biogenesis extends beyond acting exclusively in the AP-3–trafficking pathway, as *vps-18* mutants exhibit a stronger Glo phenotype than when AP-3 activity is abolished, and mutations in both *vps-18* and *vps-41* modify the Glo phenotype of AP-3 mutants (Tables 1 and 2). There are a number of ways that HOPS might promote gut granule biogenesis independent of AP-3. HOPS functions in the fusion of late endosomes and lysosomes by promoting the assembly and activity of soluble *N*-ethylmaleimide–sensitive factor attachment protein receptor (SNARE) complexes, which mediate membrane fusion (Balderhaar and Ungermann, 2013; Pols *et al.*, 2013; Solinger and Spang, 2013). SNAREs likely mediate trafficking to LROs (Ghiani *et al.*, 2010; Tamura *et al.*, 2011; Yatsu *et al.*, 2013); however, the site of SNARE action and the specific membrane fusion events that they regulate during LRO biogenesis are unknown. HOPS activity has also been implicated in the maturation of early to late endosomes by functioning to inactivate Rab5 on early endosomes, as well as to activate and recruit Rab7 on nascent late endosomes (Wang *et al.*, 2003; Rink *et al.*, 2005; Nordmann *et al.*, 2010; Poteryaev *et al.*, 2010). Organelle maturation, possibly associated with Rab conversion (Hume *et al.*, 2011), occurs during mammalian melanosome biogenesis (Sitaram and Marks, 2012). However, whether organelle maturation is a conserved feature of LRO biogenesis and whether HOPS directly facilitates this process are open questions.

Rab GTPase activity during gut granule formation

In yeast, Rab7 recruits HOPS and its associated tethering and membrane fusion activity (Price *et al.*, 2000; Wurmser *et al.*, 2000; Brett *et al.*, 2008; Plemel *et al.*, 2011). We found that HOPS mutants displayed stronger gut granule protein biogenesis and trafficking defects than did loss of RAB-7 (Figures 1–5), suggesting that HOPS activity in gut granule biogenesis only partially depends on RAB-7 and that HOPS interacts with another Rab or has Rab-independent activities.

Gut granules were formed in *rab-7* mutants (Figures 1–3 and Tables 1–2); however, their size was modestly altered (Supplemental Figure S2), and LMP-1 accumulation on nascent gut granules was disrupted (Figures 4 and 5). Similarly, Rab7 activity partially regulates the protein composition of melanosomes (Hida *et al.*, 2011). Rab7 is associated with many different mammalian LROs (Jordens *et al.*, 2006; Kawakami *et al.*, 2008; Zhang *et al.*, 2011; Ambrosio *et al.*, 2012); however, we did not detect RAB-7 on gut granules at the stage when gut granule defects were observed (Figure 6 and Supplemental Figure S2), suggesting that RAB-7 exerts its effects indirectly or at an early point in the trafficking pathway to gut granules. In addition, the different effects of *sand-1* and *rab-7* mutants on gut granule formation (Figures 4 and 5) point to an LRO-related function of RAB-7 that is independent of SAND-1/Mon1–mediated activation.

C. elegans RAB-7 mediates the trafficking between early and late endosomes (Poteryaev *et al.*, 2007), the fusion between lysosomes and cell corpse–containing phagosomes (Yu *et al.*, 2008; Guo and Wang, 2010), and yolk degradation (Grant and Hirsh, 1999; Britton and Murray, 2004). In these processes, a complex of CCZ-1 and SAND-1 likely functions as a GEF to generate active GTP-bound RAB-7 (Poteryaev *et al.*, 2007, 2010; Kinchen and Ravichandran, 2010; Nieto *et al.*, 2010; Nordmann *et al.*, 2010; Gerondopoulos *et al.*, 2012; Yousefian *et al.*, 2013). Given the subtle effects of *rab-7* mutants on gut granules, it was surprising that *ccz-1* mutants displayed significant defects in protein trafficking to gut granules

(Figures 1–5 and Tables 1 and 2), which suggests that CCZ-1 functions to activate another Rab GTPase. In this case, CCZ-1 would be expected to function upstream of the Rab. In yeast, Ccz1 acts as a GEF for Rab7 in vitro, and predicted spontaneous nucleotide exchange mutations in Rab7 bypass the requirement for Ccz1 in lysosome biogenesis, providing a genetic indicator that Ccz1 acts upstream of Rab7 (Kucharczyk *et al.*, 2001; Nordmann *et al.*, 2010; Cabrera and Ungermann, 2013). Similar mutations in GLO-1, a Rab GTPase homologous to Rab32 and Rab38 and predicted to bypass GEF activity (McCray *et al.*, 2010), restored gut granules in *ccz-1* mutants (Figure 9 and Table 3). Recent in vitro studies demonstrate that mammalian BLOC-3, composed of HPS4 and HPS1, which are homologous to CCZ-1 and SAND-1/Mon1, respectively, functions as a GEF for Rab32 and Rab38 (Gerondopoulos *et al.*, 2012). Mutations in HPS1 and HPS4 lead to Hermansky–Pudlak syndrome and display defects in the formation of LROs (Oh *et al.*, 1996; Suzuki *et al.*, 2002; Chiang *et al.*, 2003; Martina *et al.*, 2003; Nazarian *et al.*, 2003; Gerondopoulos *et al.*, 2012). Therefore, if CCZ-1 functions analogously to HPS4, it would be expected to act as a GEF for the Rab GLO-1.

sand-1 mutants did not substantially alter gut granule biogenesis (Figures 1–5 and Tables 1 and 2; Poteryaev *et al.*, 2007), in contrast to what would be predicted if CCZ-1 and SAND-1 functioned together in a complex similar to HPS4 and HPS1. We demonstrate that *C. elegans* GLO-3 exhibits significant sequence similarity with human and *Drosophila* HPS1 and SAND-1/Mon1–related proteins (Figure 9). Of note, the region of highest homology is within the Longin domain of HPS1, which mediates the interaction with HPS4 in BLOC-3 (Carmona-Rivera *et al.*, 2013), suggesting that GLO-3 functions with CCZ-1 in gut granule biogenesis. *glo-3* mutants exhibit defects in gut granule biogenesis, and GLO-3::GFP localizes to the gut granule membrane (Rabbitts *et al.*, 2008). Moreover, predicted spontaneous nucleotide exchange mutations in GLO-1 Rab restored gut granules in *glo-3* mutants (Figure 9), consistent with GLO-3 and CCZ-1 functioning similarly in gut granule biogenesis. These results suggest the interesting possibility that CCZ-1 could have dual functions, acting with GLO-3 as part of a BLOC-3–like complex upstream of the Rab GLO-1 during trafficking to gut granules, and also acting with SAND-1 to activate RAB-7 during trafficking to conventional lysosomes. However, the genetic data leave open the possibility of alternate models in which CCZ-1, GLO-3, and GLO-1 have distinct functions unrelated to each other during gut granule protein trafficking.

Mechanism of gut granule biogenesis

Lysosomes and LROs, although distinct compartments that coexist in many cell types, share a general cellular mechanism of biogenesis. For both, a precursor to the fully developed compartment matures from another organelle. This is followed by retrograde removal of material from the pre-compartment, as well as the addition of other cargo via vesicular membrane transport. Integral to these processes are Rab GTPases, their regulators, and their effectors. During lysosome biogenesis, which is much better understood than LRO formation, the early endosome matures into a late endosome that receives material from other organelles, including AP-3 pathway vesicles and mature lysosomes (Luzio *et al.*, 2007; Dell'Angelica, 2009; Marks *et al.*, 2013). Rab7, its GEF CCZ-1/SAND-1, and the Rab-7 effector HOPS play key roles in organelle maturation and membrane docking and fusion (Balderhaar and Ungermann, 2013; Solinger and Spang, 2013).

The requirement for the GLO-1 Rab and AP-3 in gut granule biogenesis originally suggested that a process analogous to lysosome biogenesis was at work during the creation of this LRO (Hermann *et al.*, 2005, 2012). Data presented here that HOPS and CCZ-1 function in gut granule formation further support this idea. Although we do not know the identity of the organelle that matures into a gut granule, there are precedents for pre-LROs emerging from the *trans*-Golgi network, early endosomes, or late endosomes (Marks *et al.*, 2013). It is unlikely that gut granule precursors develop from lysosomes, since blocking lysosome biogenesis at the endolysosome stage, immediately before the formation of mature lysosomes, does not disrupt gut granule formation (Treusch *et al.*, 2004; Campbell and Fares, 2010). SAND-1 and RAB-7 are required for normal maturation of early to late endosomes in *C. elegans* (Poteryaev *et al.*, 2007, 2010). Thus the observations that *sand-1* mutant embryos contained gut granules and *rab-7* mutant embryos had nearly normal gut granules suggest that late endosomes do not significantly contribute to gut granule biogenesis and that early to late endosome maturation is not a major contributor to gut granule biogenesis. Gut granules are accessible to externally applied endocytic tracers (Clokey and Jacobson, 1986; Hermann *et al.*, 2005), supporting the possibility that the pre–gut granule emerges from the early endosome rather than the *trans*-Golgi network. Possibly the CDF-2::GFP compartments that accumulate in *ccz-1* mutants, which lack known gut granule and lysosomal proteins (Figures 2–5), represent a pre-LRO derived from the early endosome. In any case, our genetic studies suggest a model in which CCZ-1 and GLO-3 act as upstream activators of the GLO-1 Rab, which could function in the maturation of the pre–gut granule and recruit HOPS to regulate membrane fusion events between the pre-LRO and other organelles, such as those generated by AP-3. Additional studies are needed to test this idea and define the precise cellular and molecular processes that mediate gut granule formation. This work will not only provide insights into LRO biogenesis, but will also illuminate the key similarities and differences between lysosome and LRO biogenesis.

MATERIALS AND METHODS

Nematode strains and culture

C. elegans strains were grown at 22°C, unless noted, on NGM media seeded with OP50 bacteria as described (Stiernagle, 2006). N2 was used as the wild-type strain. In standard *C. elegans* nomenclature, gene names are written in lowercase italics and if appropriate followed by a mutant allele placed in parentheses, and proteins are written in all capitals. The following mutant alleles contained within the N2 background were used: *apt-6(ok429)*, *apt-7(tm920)*, *arl-8(tm2504)*, *ccz-1(ok2182)*, *ccz-1(t2129)*, *glo-1(zu437)*, *glo-2(tm592)*, *glo-2(zu455)*, *glo-3(kx90)*, *glo-3(kx94)*, *glo-4(ok623)*, *him-5(e1490)*, *pgp-2(kx48)*, *rab-7(ok511)*, *sand-1(ok1963)*, *sand-1(or552)*, *snpn-1(tm1892)*, *vps-8(ok2912)*, *vps-11(ok1664)*, *vps-16(ok719)*, *vps-16(ok776)*, *vps-18(tm1125)*, *vps-33.1(ok2494)*, *vps-39(ok2442)*, *vps-39(tm2253)*, *vps-41(ep402)*, *vps-41(ok3433)*, and *vps-45(tm246)*. The following transgenes were used: *amIs2[cdf-2::gfp; unc-119(+)]I*, *amIs4[cdf-2::gfp; unc-119(+)]*, *jcpEx2[ced-1p::ccz-1::yfp; unc-119(+); myo-2::GFP]*, *kxEx148[F11E6.1::mCherry; Rol-6^{D}]*, *kxEx247[vha-6p::gfp::glo-1; Rol-6^{D}]*, *kxEx249[vha-6p::gfp::glo-1(K130E); Rol-6^{D}]*, *kxEx252[vha-6p::gfp::glo-1(D132A); Rol-6^{D}]*, *kxEx254[vha-6p::gfp::glo-1(I133F); Rol-6^{D}]*, *pwIs50[lmp-1p::lmp-1::gfp; unc-119(+)]*, *pwEx31[lmp-1p::lmp-1::gfp; unc-119(+)]*, and *yqEx115[vps-18p::vps-18::gfp; unc-76(+)]*. The strains and alleles are described at WormBase (www.wormbase.org).

Genetic manipulations

Using standard genetic approaches, we found that the embryonic Glo phenotype of *vps-18(tm1125)* was recessively expressed and

maternally and zygotically rescued. Introduction of a *vps-18::gfp* transgene whose expression is typically silenced in the germline (Kelly *et al.*, 1997) rescued the embryonic Glo phenotype of *vps-18(-)*, suggesting that embryonic expression is sufficient for *vps-18(+)* function in gut granule biogenesis. The presence of the *vps-18(tm1125)* deletion was verified by PCR and DNA sequencing. The Glo phenotype of *ccz-1(ok2182)* and *ccz-1(t2129)* embryos was recessively expressed and maternally and zygotically rescued. The adult Glo phenotype of these *ccz-1* alleles, although recessive, was not maternally rescued. Introduction of a *ccz-1::yfp* transgene whose expression is controlled by the *ced-1* promoter rescued the embryonic Glo phenotype of *ccz-1(-)*, suggesting that embryonic expression is sufficient for *ccz-1(+)* function in gut granule biogenesis.

Genetic crosses were used to introduce and make homozygous the integrated *cdf-2::gfp* and *lmp-1::gfp* transgenes in different mutant backgrounds. Owing to linkage of *pwIs50* and *sand-1*, *sand-1(or552)* was crossed into a strain containing the extrachromosomal *pwEx31*[*lmp-1::gfp*] transgene. The *ccz-1(-)* and *vps-18(-)* mutants were made homozygous after crossing into a *kxEx148*[*F11E6.1::mCherry; Rol-6^{D}*]–containing strain. The mutations being examined for effects on protein trafficking were homozygous except for *rab-7(ok511)* and some *ccz-1(ok2182)*–containing strains, which were maintained as heterozygotes. Homozygous *rab-7(-)* and *ccz-1(-)* individuals were identified by the presence of large refractile organelles visible by differential interference contrast (DIC) microscopy.

apt(-); him-5(-) males were typically used to generate *apt-6(-)* and *apt-7(-)*–containing double mutants. From crosses of *apt(-)* with *vps-18(-)*, resulting F2 adults that exhibited wild-type autofluorescence and corresponding F3 Glo embryos were isolated. These F3s were then cloned out to identify lines exhibiting the *apt(-)* Glo phenotype upon reaching adulthood. In crosses with *vps-41(-)* and *apt-6(-)*, the *apt-6(-)* allele was marked by a closely linked *dpy-5(-)* mutation, and *vps-41(-)* was marked by a closely linked *unc-6(-)* mutation. Dpy Unc F2 offspring of the cross were isolated and scored. From crosses of *apt(-)* with *ccz-1(-)* and *sand-1(-)*, resulting F2 progeny that exhibited the *apt(-)* adult Glo phenotype, which lacked early-stage embryos with large refractile organelles indicative of *ccz-1(-)* and *sand-1(-)*, were isolated. F3 progeny were cloned out, and those producing embryos with refractile organelles were isolated. From crosses of *apt(-)* and other *glo(-)* mutants with *rab-7(-)*, resulting F2 adult progeny exhibiting a Glo phenotype were isolated and allowed to self. Resulting F3 animals that laid *rab-7(-)* dead embryos were scored. In all cases multiple double-mutant lines were isolated and scored.

RNAi feeding protocol 1 (Kamath *et al.*, 2001), using bacterial clones from the Ahringer RNAi library (available from Source Bioscience, Nottingham, United Kingdom) or, when these were not present for the gene being studied, the Vidal RNAi library (available from Thermo Scientific, Pittsburgh, PA), was used to knock down gene expression. In some cases *rrf-3(pk1426)* was used (Simmer *et al.*, 2003). Briefly, gravid adults were bleached to isolate embryos, which were placed onto freshly seeded RNAi plates. When these embryos developed to adulthood, they and their resulting embryonic progeny were scored unless otherwise stated.

Generating GLO-1(ΔG4) mutants

The G4 domain of GLO-1 was altered using site-directed mutagenesis with QuikChange II (Agilent Technologies, Santa Clara, CA) and a *vha-6p::gfp::glo-1::let-858 3′UTR* plasmid as a template (Hermann *et al.*, 2005). Primers p868, 5′CCAGCAATTTTACTTGCAAACGAGTGTGATATCGACAATAAAC3′, and p869, 5′GTTTATTGTCGATATCACACTCGTTTGCAAGTAAAATTGCTGG3′, were used to generate GLO-1(K130E).

Primers P870, 5′CTTGCAAACAAGTGTGCTATCGACAATAAACTTGGTGACG3′, and P871, 5′CGTCACCAAGTTTATTGTCGATAGCACACTTGTTTGCAAG3′, were used to generate GLO-1(D132A).

Primers P872, 5′CTTGCAAACAAGTGTGATTTCGACAATAACTTGGTGACG3′, and P873, 5′CGTCACCAAGTTATTGTCGAAATCACACTTGTTTGCAAG3′, were used to generate GLO-1(I133F). Underlined residues denote point mutations. For each mutagenized construct, the coding sequence of *gfp::glo-1* was sequenced at the Oregon Health & Science University DNA Services Core facility (Portland, OR) to verify that only the desired point mutation had been introduced. The wild-type *vha-6p::gfp::glo-1* plasmid and the three *glo-1(ΔG4)* mutant constructs were individually coinjected at 1 ng/μl with pRF4 [Rol-6^{D}] at 100 ng/μl into *glo-1(zu437)*. The resulting transmitting lines with similar expression of GFP::GLO-1 were characterized. Each of the extrachromosomal arrays was assessed for restoration of adult autofluorescent compartments and then moved via a genetic cross into a wild-type background. The arrays did not dominantly alter the number of autofluorescent compartments in wild type. The arrays were crossed from wild type into different *glo*- mutant backgrounds to generate the analyzed strains.

Microscopy

A Zeiss AxioImager.M2 microscope equipped with DIC, polarization, and fluorescence optics was used for all imaging (Zeiss, Thornwood, NY). Images were captured using an AxioCam MRm digital camera controlled with AxioVision 4.8 software. In all cases, optical *Z*-series through the regions of interest were captured, and, as indicated in the figure legends, individual optical sections or maximum intensity projections are presented.

L4-stage larvae and adults were immobilized on 3% agarose pads for imaging by mounting animals in 10 mM levamisole (Sigma-Aldrich, St. Louis, MO) or 0.1 μm polystyrene nanobeads (Polysciences, Warrington, PA). Autofluorescent gut granules were visualized with Zeiss 38 (GFP, excitation, BP 470/40; emission, BP 525/50), Zeiss 45 (mCherry; excitation, BP 560/40; emission, BP 630/75), or Zeiss 49 (4′,6-diamidino-2-phenylindole [DAPI]; excitation, G 365; emission, 445/50) filters. Acidic compartments within adults were stained with acridine orange (Sigma-Aldrich) as described (Hermann *et al.*, 2005) and visualized with a Zeiss 45 filter. For each strain, a camera exposure time was identified that did not reveal endogenous autofluorescence in unstained animals, which was used to image acridine orange–stained compartments. *ccz-1(ok2182)/+* animals containing *gfp::glo-1* or *gfp::glo-1(ΔG4)* transgenes were maintained, and resulting homozygous *ccz-1(-)* adult progeny with the transgene, which were scored, were identified by both the presence of early-stage embryos with large refractile organelles indicative of *ccz-1(-)* and the intestinal expression of GFP. In all lines, *ccz-1(-)* animals lacking GFP expression exhibited a Glo phenotype.

Living embryos were mounted on 3% agarose pads in H_2O or 1XM9 for imaging. To immobilize living pretzel-stage animals, excess respiring OP50 bacteria were added with the embryos to induce hypoxia. Within embryos, birefringent material was visualized with polarization optics, and autofluorescent compartments were visualized with a Zeiss 49 filter, LMP-1::GFP was visualized with a Zeiss 38 filter, and F11E6.1a::mCherry was visualized with a Zeiss 45 filter. The number of LMP-1::GFP–containing compartments was scored using *Z*-stacks spanning the entire intestine of 1.5-fold-stage embryos fixed with 100% MeOH to prevent the movement of organelles. LMP-1::GFP is enriched on the plasma membrane of

intestinal cells, enabling the identification of the four cells that compose Int2 and Int3 (Leung *et al.*, 1999) and the quantification of the number of LMP-1::GFP compartments contained within these cells. Acidified compartments within embryos were stained with LysoSensor Green (Invitrogen, Grand Island, NY) as described (Levitte *et al.*, 2010) and imaged with a Zeiss 38 filter.

Embryos were fixed and stained with LMP-1 (Hadwiger *et al.*, 2010), PGP-2 (Schroeder *et al.*, 2007), RAB-5 (Audhya *et al.*, 2007), and RAB-7 (Chen *et al.*, 2010) antibodies as described (Leung *et al.*, 1999). The specificity of these antisera using the staining protocol was confirmed in prior work. This protocol extracts the autofluorescent material present within embryonic gut granules. GFP fluorescence was used to visualize CDF-2::GFP and LMP-1::GFP in antibody-stained embryos. Because *rab-7(-)* causes maternal effect lethality, homozygous *rab-7(-)* embryos derived from homozygous *rab-7(-)* hermaphrodites were identified in mixed populations by their altered 1.5-fold body morphology and enlarged PGP-2 or CDF-2::GFP– marked gut granules. For colocalization studies, two-channel *Z*-stacks containing signals identifying different organelle associated proteins were acquired and analyzed. For each of the five 1.5-fold-stage embryos in each experiment, 25–35 organelles containing the protein of interest were randomly selected from within the intestine, and each was manually scored for the presence/colocalization of the other marker. If the signals marking the two proteins overlapped, they were scored as colocalizing. Statistical analysis, which is described in the figure legends, was carried out using Excel 2010 (Microsoft, Redmond, WA).

The images presented are representative of the data used to quantify number, size, and colocalization. The figures were prepared using Photoshop CS2 (Adobe, San Jose, CA), and only contrast was adjusted.

Bioinformatics

Default settings were used in PSI-BLAST searches (Altschul *et al.*, 1997). The location of β-strands and α-helices in the Longin domain of HPS1 are from homology-based structural predictions (Kinch and Grishin, 2006). Secondary structure predictions of GLO-3 were generated using JPRED (Cole *et al.*, 2008), PHD (Przybylski and Rost, 2002), and PSIPRED (Jones, 1999) algorithms.

ACKNOWLEDGMENTS

We are grateful to Juan Cabello, Barth Grant, Anne Spang, and Chonglin Yang for strains. We thank Peter Kennedy and Teri Peterson for assistance with statistical analysis. We acknowledge Lewis & Clark Bio361 students from 2006, 2010, and 2011 for carrying out the initial studies of *ccz-1*, *sand-1*, and *vps-18* mutants. Some strains were provided by the *Caenorhabditis* Genetics Center, which is funded by National Institutes of Health Office of Research Infrastructure Program P40 OD010440, the *C. elegans* Knockout Consortium, and the National Bioresource Project for *C. elegans*. This work was supported by the National Science Foundation (MCB-1120835), the James F. and Marion L. Miller Foundation, and the John S. Rogers Summer Research Program.

REFERENCES

Akbar MA, Ray S, Kramer H (2009). The SM protein Car/Vps33A regulates SNARE-mediated trafficking to lysosomes and lysosome-related organelles. Mol Biol Cell 20, 1705–1714.

Altschul SF, Madden TL, Schaffer AA, Zhang J, Zhang Z, Miller W, Lipman DJ (1997). Gapped BLAST and PSI-BLAST: a new generation of protein database search programs. Nucleic Acids Res 25, 3389–3402.

Ambrosio AL, Boyle JA, Di Pietro SM (2012). Mechanism of platelet dense granule biogenesis: study of cargo transport and function of Rab32 and Rab38 in a model system. Blood 120, 4072–4081.

Angers CG, Merz AJ (2009). HOPS interacts with Apl5 at the vacuole membrane and is required for consumption of AP-3 transport vesicles. Mol Biol Cell 20, 4563–4574.

Aoyama M, Sun-Wada GH, Yamamoto A, Yamamoto M, Hamada H, Wada Y (2012). Spatial restriction of bone morphogenetic protein signaling in mouse gastrula through the mVam2-dependent endocytic pathway. Dev Cell 22, 1163–1175.

Audhya A, Desai A, Oegema K (2007). A role for Rab5 in structuring the endoplasmic reticulum. J Cell Biol 178, 43–56.

Balderhaar HJ, Ungermann C (2013). CORVET and HOPS tethering complexes—coordinators of endosome and lysosome fusion. J Cell Sci 126, 1307–1316.

Bossinger O, Schierenberg E (1992). Transfer and tissue-specific accumulation of cytoplasmic components in embryos of *Caenorhabditis elegans* and *Rabditis dolichura*: in vivo analysis with a low-cost signal enhancement device. Development 114, 317–330.

Brett CL, Plemel RL, Lobingier BT, Vignali M, Fields S, Merz AJ (2008). Efficient termination of vacuolar Rab GTPase signaling requires coordinated action by a GAP and a protein kinase. J Cell Biol 182, 1141–1151.

Bright NA, Gratian MJ, Luzio JP (2005). Endocytic delivery to lysosomes mediated by concurrent fusion and kissing events in living cells. Curr Biol 15, 360–365.

Britton C, Murray L (2004). Cathepsin L protease (CPL-1) is essential for yolk processing during embryogenesis in *Caenorhabditis elegans*. J Cell Sci 117, 5133–5143.

Cabrera M *et al.* (2010). Phosphorylation of a membrane curvature-sensing motif switches function of the HOPS subunit Vps41 in membrane tethering. J Cell Biol 191, 845–859.

Cabrera M, Ungermann C (2013). Guanine nucleotide exchange factors (GEFs) have a critical but not exclusive role in organelle localization of Rab GTPases. J Biol Chem 288, 28704.

Campbell EM, Fares H (2010). Roles of CUP-5, the *Caenorhabditis elegans* orthologue of human TRPML1, in lysosome and gut granule biogenesis. BMC Cell Biol 11, 40.

Caplan S, Hartnell LM, Aguilar RC, Naslavsky N, Bonifacino JS (2001). Human Vam6p promotes lysosome clustering and fusion in vivo. J Cell Biol 154, 109–122.

Carmona-Rivera C, Simeonov DR, Cardillo ND, Gahl WA, Cadilla CL (2013). A divalent interaction between HPS1 and HPS4 is required for the formation of the biogenesis of lysosome-related organelle complex-3 (BLOC-3). Biochim Biophys Acta 1833, 468–478.

Chen B, Jiang Y, Zeng S, Yan J, Li X, Zhang Y, Zou W, Wang X (2010). Endocytic sorting and recycling require membrane phosphatidylserine asymmetry maintained by TAT-1/CHAT-1. PLoS Genet 6, e1001235.

Chiang PW, Oiso N, Gautam R, Suzuki T, Swank RT, Spritz RA (2003). The Hermansky-Pudlak syndrome 1 (HPS1) and HPS4 proteins are components of two complexes, BLOC-3 and BLOC-4, involved in the biogenesis of lysosome-related organelles. J Biol Chem 278, 20332–20337.

Clokey GV, Jacobson LA (1986). The autofluorescent "lipofuscin granules" in the intestinal cells of *Caenorhabditis elegans* are secondary lysosomes. Mech Ageing Dev 35, 79–94.

Coburn C *et al.* (2013). Anthranilate fluorescence marks a calcium-propagated necrotic wave that promotes organismal death in *C. elegans*. PLoS Biol 11, e1001613.

Cole C, Barber JD, Barton GJ (2008). The Jpred 3 secondary structure prediction server. Nucleic Acids Res 36, W197–W201.

Collins BM, McCoy AJ, Kent HM, Evans PR, Owen DJ (2002). Molecular architecture and functional model of the endocytic AP2 complex. Cell 109, 523–535.

Darsow T, Katzmann DJ, Cowles CR, Emr SD (2001). Vps41p function in the alkaline phosphatase pathway requires homo-oligomerization and interaction with AP-3 through two distinct domains. Mol Biol Cell 12, 37–51.

Davis DE, Roh HC, Deshmukh K, Bruinsma JJ, Schneider DL, Guthrie J, Robertson JD, Kornfeld K (2009). The cation diffusion facilitator gene *cdf-2* mediates zinc metabolism in *Caenorhabditis elegans*. Genetics 182, 1015–1033.

De Franceschi N, Wild K, Schlacht A, Dacks JB, Sinning I, Filippini F (2014). Longin and GAF domains: structural evolution and adaptation to the subcellular trafficking machinery. Traffic 15, 104–121.

Dell'Angelica EC (2009). AP-3-dependent trafficking and disease: the first decade. Curr Opin Cell Biol 21, 552–559.

Dell'Angelica EC, Mullins C, Caplan S, Bonifacino JS (2000). Lysosome-related organelles. FASEB 14, 1265–1278.

Dell'Angelica EC, Shotelersuk V, Aguilar RC, Gahl WA, Bonifacino JS (1999). Altered trafficking of lysosomal proteins in Hermansky-Pudlak syndrome

due to mutations in the b3A subunit of the AP-3 adaptor. Mol Cell 3, 11–21.
Di Pietro SM, Falcon-Perez JM, Tenza D, Setty SR, Marks MS, Raposo G, Dell'Angelica EC (2006). BLOC-1 interacts with BLOC-2 and the AP-3 complex to facilitate protein trafficking on endosomes. Mol Biol Cell 17, 4027–4038.
Docampo R, Ulrich P, Moreno SN (2010). Evolution of acidocalcisomes and their role in polyphosphate storage and osmoregulation in eukaryotic microbes. Philos Trans R Soc Lond B Biol Sci 365, 775–784.
Epp N, Rethmeier R, Kramer L, Ungermann C (2011). Membrane dynamics and fusion at late endosomes and vacuoles—Rab regulation, multisubunit tethering complexes and SNAREs. Eur J Cell Biol 90, 779–785.
Feng L *et al.* (1999). The beta3A subunit gene (Ap3b1) of the AP-3 adaptor complex is altered in the mouse hypopigmentation mutant pearl, a model for Hermansky-Pudlak syndrome and night blindness. Hum Mol Genet 8, 323–330.
Filippini F, Rossi V, Galli T, Budillon A, D'Urso M, D'Esposito M (2001). Longins: a new evolutionary conserved VAMP family sharing a novel SNARE domain. Trends Biochem Sci 26, 407–409.
Gallegos ME *et al.* (2012). The *C. elegans* Rab family: identification, classification and toolkit construction. PLoS One 7, e49387.
Garg S, Sharma M, Ung C, Tuli A, Barral DC, Hava DL, Veerapen N, Besra GS, Hacohen N, Brenner MB (2011). Lysosomal trafficking, antigen presentation, and microbial killing are controlled by the Arf-like GTPase Arl8b. Immunity 35, 182–193.
Gerondopoulos A, Langemeyer L, Liang JR, Linford A, Barr FA (2012). BLOC-3 mutated in Hermansky-Pudlak syndrome is a Rab32/38 guanine nucleotide exchange factor. Curr Biol 22, 2135–2139.
Ghiani CA, Starcevic M, Rodriguez-Fernandez IA, Nazarian R, Cheli VT, Chan LN, Malvar JS, de Vellis J, Sabatti C, Dell'Angelica EC (2010). The dysbindin-containing complex (BLOC-1) in brain: developmental regulation, interaction with SNARE proteins and role in neurite outgrowth. Mol Psychiatry 15, 204–115.
Graham SC, Wartosch L, Gray SR, Scourfield EJ, Deane JE, Luzio JP, Owen DJ (2013). Structural basis of Vps33A recruitment to the human HOPS complex by Vps16. Proc Natl Acad Sci USA 110, 13345–13350.
Grant B, Hirsh D (1999). Receptor-mediated endocytosis in the *Caenorhabditis elegans* oocyte. Mol Biol Cell 10, 4311–4326.
Guo P, Wang X (2010). Rab GTPases act in sequential steps to regulate phagolysosome formation. Small GTPases 1, 170–173.
Hadwiger G, Dour S, Arur S, Fox P, Nonet ML (2010). A monoclonal antibody toolkit for *C. elegans*. PLoS One 5, e10161.
Hermann GJ *et al.* (2012). *C. elegans* BLOC-1 functions in trafficking to lysosome-related gut granules. PLoS One 7, e43043.
Hermann GJ, Schroeder LK, Hieb CA, Kershner AM, Rabbitts BM, Fonarev P, Grant BD, Priess JR (2005). Genetic analysis of lysosomal trafficking in *Caenorhabditis elegans*. Mol Biol Cell 16, 3273–3288.
Hershkovitz D, Mandel H, Ishida-Yamamoto A, Chefetz I, Hino B, Luder A, Indelman M, Bergman R, Sprecher E (2008). Defective lamellar granule secretion in arthrogryposis, renal dysfunction, and cholestasis syndrome caused by a mutation in VPS33B. Arch Dermatol 144, 334–340.
Hickey CM, Wickner W (2010). HOPS initiates vacuole docking by tethering membranes before trans-SNARE complex assembly. Mol Biol Cell 21, 2297–2305.
Hida T, Sohma H, Kokai Y, Kawakami A, Hirosaki K, Okura M, Tosa N, Yamashita T, Jimbow K (2011). Rab7 is a critical mediator in vesicular transport of tyrosinase-related protein 1 in melanocytes. J Dermatol 38, 432–441.
Hirosaki K, Yamashita T, Wada I, Jin HY, Jimbow K (2002). Tyrosinase and tyrosinase-related protein 1 require Rab7 for their intracellular transport. J Invest Dermatol 119, 475–480.
Hoffman-Sommer M, Grynberg M, Kucharczyk R, Rytka J (2005). The CHiPS domain—ancient traces for the Hermansky-Pudlak syndrome. Traffic 6, 534–538.
Huizing M, Helip-Wooley A, Westbroek W, Gunay-Aygun M, Gahl WA (2008). Disorders of lysosome-related organelle biogenesis: clinical and molecular genetics. Annu Rev Genomics Hum Genet 9, 359–386.
Huizing M, Sarangarajan R, Stroval E, Zhou Y, Gahl WA, Boissy RE (2001). AP-3 mediates tyrosinase but not TRP-1 trafficking in human melanocytes. Mol Biol Cell 12, 2075–2085.
Hume AN, Wilson MS, Ushakov DS, Ferenczi MA, Seabra MC (2011). Semi-automated analysis of organelle movement and membrane content: understanding Rab-motor complex transport function. Traffic 12, 1686–1701.
Jones DT (1999). Protein secondary structure prediction based on position-specific scoring matrices. J Mol Biol 292, 195–202.
Jordens I, Westbroek W, Marsman M, Rocha N, Mommaas M, Huizing M, Lambert J, Naeyaert JM, Neefjes J (2006). Rab7 and Rab27a control two motor protein activities involved in melanosomal transport. Pigment Cell Res 19, 412–423.
Kamath RS, Martinez-Campos M, Zipperlen P, Fraser AG, Ahringer J (2001). Effectiveness of specific RNA-mediated interference through ingested double-stranded RNA in *Caenorhabditis elegans*. Genome Biol 2, RESEARCH0002.
Kantheti P *et al.* (1998). Mutation in AP-3 delta in the mocha mouse links endosomal transport to storage deficiency in platelets, melanosomes, and synaptic vesicles. Neuron 21, 111–122.
Kawakami A *et al.* (2008). Rab7 regulates maturation of melanosomal matrix protein gp100/Pmel17/Silv. J Invest Dermatol 128, 143–150.
Kelly WG, Xu S, Montgomery MK, Fire A (1997). Distinct requirements for somatic and germline expression of a generally expressed *Caenorhabditis elegans* gene. Genetics 146, 227–238.
Kim YG, Raunser S, Munger C, Wagner J, Song YL, Cygler M, Walz T, Oh BH, Sacher M (2006). The architecture of the multisubunit TRAPP I complex suggests a model for vesicle tethering. Cell 127, 817–830.
Kinchen JM, Doukoumetzidis K, Almendinger J, Stergiou L, Tosello-Trampont A, Sifri CD, Hengartner MO, Ravichandran KS (2008). A pathway for phagosome maturation during engulfment of apoptotic cells. Nat Cell Biol 10, 556–566.
Kinchen JM, Ravichandran KS (2010). Identification of two evolutionarily conserved genes regulating processing of engulfed apoptotic cells. Nature 464, 778–782.
Kinch LN, Grishin NV (2006). Longin-like folds identified in CHiPS and DUF254 proteins: vesicle trafficking complexes conserved in eukaryotic evolution. Protein Sci 15, 2669–2674.
Klopper TH, Kienle N, Fasshauer D, Munro S (2012). Untangling the evolution of Rab G proteins: implications of a comprehensive genomic analysis. BMC Biol 10, 71.
Kretzschmar D, Poeck B, Roth H, Ernst R, Keller A, Porsch M, Strauss R, Pflugfelder GO (2000). Defective pigment granule biogenesis and aberrant behavior caused by mutations in the *Drosophila* AP-3beta adaptin gene ruby. Genetics 155, 213–223.
Kucharczyk R, Kierzek AM, Slonimski PP, Rytka J (2001). The Ccz1 protein interacts with Ypt7 GTPase during fusion of multiple transport intermediates with the vacuole in *S. cerevisiae*. J Cell Sci 114, 3137–3145.
Laufer JS, Bazzicalupo P, Wood WB (1980). Segregation of developmental potential in early embryos of *Caenorhabditis elegans*. Cell 19, 569–577.
Lee YS *et al.* (2009). Silencing by small RNAs is linked to endosomal trafficking. Nat Cell Biol 11, 1150–1156.
Leung B, Hermann GJ, Priess JR (1999). Organogenesis of the *Caenorhabditis elegans* intestine. Dev Biol 216, 114–134.
Levine TP, Daniels RD, Wong LH, Gatta AT, Gerondopoulos A, Barr FA (2013). Discovery of new Longin and Roadblock domains that form platforms for small GTPases in Ragulator and TRAPP-II. Small GTPases 4, 62–69.
Levitte S, Salesky R, King B, Coe Smith S, Depper M, Cole M, Hermann GJ (2010). A *Caenorhabditis elegans* model of orotic aciduria reveals enlarged lysosome-related organelles in embryos lacking *umps-1* function. FEBS J 277, 1420–1439.
Lloyd V, Ramaswami M, Kramer H (1998). Not just pretty eyes: *Drosophila* eye color mutations and lysosomal delivery. Trends Cell Biol 8, 257–259.
Lo B *et al.* (2005). Requirement of VPS33B, a member of the Sec1/Munc18 protein family, in megakaryocyte and platelet alpha-granule biogenesis. Blood 106, 4159–4166.
Luzio JP, Pryor PR, Bright NA (2007). Lysosomes: fusion and function. Nat Rev Mol Cell Biol 8, 622–632.
Ma J, Plesken H, Treisman JE, Edelman-Novemsky I, Ren M (2004). Lightoid and Claret: a Rab GTPase and its putative guanine nucleotide exchange factor in biogenesis of *Drosophila* eye pigment granules. Proc Natl Acad Sci USA 101, 11652–11657.
Mak HY, Nelson LS, Basson M, Johnson CD, Ruvkun G (2006). Polygenic control of *Caenorhabditis elegans* fat storage. Nat Genet 38, 363–368.
Maldonado E, Hernandez F, Lozano C, Castro ME, Navarro RE (2006). The zebrafish mutant vps18 as a model for vesicle-traffic related hypopigmentation diseases. Pigment Cell Res 19, 315–326.
Marat AL, Dokainish H, McPherson PS (2011). DENN domain proteins: regulators of Rab GTPases. J Biol Chem 286, 13791–13800.
Marks MS, Heijnen HF, Raposo G (2013). Lysosome-related organelles: unusual compartments become mainstream. Curr Opin Cell Biol 25, 495–505.

Martina JA, Moriyama K, Bonifacino JS (2003). BLOC-3, a protein complex containing the Hermansky-Pudlak syndrome gene products HPS1 and HPS4. J Biol Chem 278, 29376–29384.
Matthews RP, Plumb-Rudewiez N, Lorent K, Gissen P, Johnson CA, Lemaigre F, Pack M (2005). Zebrafish vps33b, an ortholog of the gene responsible for human arthrogryposis-renal dysfunction-cholestasis syndrome, regulates biliary development downstream of the onecut transcription factor hnf6. Development 132, 5295–5306.
McCray BA, Skordalakes E, Taylor JP (2010). Disease mutations in Rab7 result in unregulated nucleotide exchange and inappropriate activation. Hum Mol Genet 19, 1033–1047.
Messler S *et al.* (2011). The TGF-beta signaling modulators TRAP1/TGF-BRAP1 and VPS39/Vam6/TLP are essential for early embryonic development. Immunobiology 216, 343–350.
Mullins C, Hartnell LM, Bonifacino JS (2000). Distinct requirements for the AP-3 adaptor complex in pigment granule and synaptic vesicle biogenesis in *Drosophila melanogaster*. Mol Gen Genet 263, 1003–1014.
Mullins C, Hartnell LM, Wassarman DA, Bonifacino JS (1999). Defective expression of the mu3 subunit of the AP-3 adaptor complex in the *Drosophila* pigmentation mutant carmine. Mol Gen Genet 262, 401–412.
Nakae I, Fujino T, Kobayashi T, Sasaki A, Kikko Y, Fukuyama M, Gengyo-Ando K, Mitani S, Kontani K, Katada T (2010). The Arf-like GTPase Arl8 mediates delivery of endocytosed macromolecules to lysosomes in *Caenorhabditis elegans*. Mol Biol Cell 21, 2434–2442.
Nazarian R, Falcon-Perez JM, Dell'Angelica EC (2003). Biogenesis of lysosome-related organelles complex 3 (BLOC-3): a complex containing the Hermansky-Pudlak syndrome (HPS) proteins HPS1 and HPS4. Proc Natl Acad Sci USA 100, 8770–8775.
Nguyen T, Wei ML (2004). Characterization of melanosomes in murine Hermansky-Pudlak syndrome: mechanisms of hypopigmentation. J Invest Dermatol 122, 452–460.
Nickerson DP, Brett CL, Merz AJ (2009). Vps-C complexes: gatekeepers of endolysosomal traffic. Curr Opin Cell Biol 21, 543–551.
Nieto C, Almendinger J, Gysi S, Gomez-Orte E, Kaech A, Hengartner MO, Schnabel R, Moreno S, Cabello J (2010). ccz-1 mediates the digestion of apoptotic corpses in *C. elegans*. J Cell Sci 123, 2001–2007.
Nordmann M, Cabrera M, Perz A, Brocker C, Ostrowicz C, Engelbrecht-Vandre S, Ungermann C (2010). The Mon1-Ccz1 complex is the GEF of the late endosomal Rab7 homolog Ypt7. Curr Biol 20, 1654–1659.
Oh J, Bailin T, Fukai K, Feng GH, Ho L, Mao JI, Frenk E, Tamura N, Spritz RA (1996). Positional cloning of a gene for Hermansky-Pudlak syndrome, a disorder of cytoplasmic organelles. Nat Genet 14, 300–306.
Oka T, Toyomura T, Honjo K, Wada Y, Futai M (2001). Four subunit *a* isoforms of *Caenorhabditis elegans* vacuolar H^+-ATPase. J Biol Chem 276, 3309–33085.
Ooi CE, Moreira JE, Dell'Angelica EC, Poy G, Wassarman DA, Bonifacino JS (1997). Altered expression of a novel adaptin leads to defective pigment granule biogenesis in the *Drosophila* eye color mutant garnet. EMBO J 16, 4508–4518.
O'Rourke EJ, Ruvkun G (2013). MXL-3 and HLH-30 transcriptionally link lipolysis and autophagy to nutrient availability. Nat Cell Biol 15, 668–676.
O'Rourke EJ, Soukas AA, Carr CE, Ruvkun G (2009). *C. elegans* major fats are stored in vesicles distinct from lysosome-related organelles. Cell Metab 10, 430–435.
Ostrowicz CW, Brocker C, Ahnert F, Nordmann M, Lachmann J, Peplowska K, Perz A, Auffarth K, Engelbrecht-Vandre S, Ungermann C (2010). Defined subunit arrangement and Rab interactions are required for functionality of the HOPS tethering complex. Traffic 11, 1334–1346.
Peng C *et al.* (2012). Ablation of vacuole protein sorting 18 (Vps18) gene leads to neurodegeneration and impaired neuronal migration by disrupting multiple vesicle transport pathways to lysosomes. J Biol Chem 287, 32861–32873.
Peplowska K, Markgraf DF, Ostrowicz CW, Bange G, Ungermann C (2007). The CORVET tethering complex interacts with the yeast Rab5 homolog Vps21 and is involved in endo-lysosomal biogenesis. Dev Cell 12, 739–750.
Plemel RL, Lobingier BT, Brett CL, Angers CG, Nickerson DP, Paulsel A, Sprague D, Merz AJ (2011). Subunit organization and Rab interactions of Vps-C protein complexes that control endolysosomal membrane traffic. Mol Biol Cell 22, 1353–1363.
Pols MS, ten Brink C, Gosavi P, Oorschot V, Klumperman J (2013). The HOPS proteins hVps41 and hVps39 are required for homotypic and heterotypic late endosome fusion. Traffic 14, 219–232.
Poteryaev D, Datta S, Ackema K, Zerial M, Spang A (2010). Identification of the switch in early-to-late endosome transition. Cell 141, 497–508.
Poteryaev D, Fares H, Bowerman B, Spang A (2007). *Caenorhabditis elegans* SAND-1 is essential for RAB-7 function in endosomal traffic. EMBO J 26, 301–312.
Price A, Seals D, Wickner W, Ungermann C (2000). The docking stage of yeast vacuole fusion requires the transfer of proteins from a cis-SNARE complex to a Rab/Ypt protein. J Cell Biol 148, 1231–1238.
Pryor PR, Mullock BM, Bright NA, Gray SR, Luzio JP (2000). The role of intraorganellar Ca(2+) in late endosome-lysosome heterotypic fusion and in the reformation of lysosomes from hybrid organelles. J Cell Biol 149, 1053–1062.
Przybylski D, Rost B (2002). Alignments grow, secondary structure prediction improves. Proteins 46, 197–205.
Pujol N, Bonnerot C, Ewbank JJ, Kohara Y, Thierry-Mieg D (2001). The *Caenorhabditis elegans unc-32* gene encodes alternative forms of a vacuolar ATPase a subunit. J Biol Chem 276, 11913–11921.
Pulipparacharuvil S, Akbar MA, Ray S, Sevrioukov EA, Haberman AS, Rohrer J, Kramer H (2005). *Drosophila* Vps16A is required for trafficking to lysosomes and biogenesis of pigment granules. J Cell Sci 118, 3663–3673.
Rabbitts BM, Kokes M, Miller NE, Kramer M, Lawrenson AL, Levitte S, Kremer S, Kwan E, Weis AM, Hermann GJ (2008). *glo-3*, a novel *Caenorhabditis elegans* gene, is required for lysosome-related organelle biogenesis. Genetics 180, 857–871.
Raposo G, Marks MS, Cutler DF (2007). Lysosome-related organelles: driving post-Golgi compartments into specialisation. Curr Opin Cell Biol 394–401.
Richardson SCW, Winistorfer SC, Poupon V, Luzio JP, Piper RC (2004). Mammalian late vacuole protein sorting orthologues participate in early endosomal fusion and interact with the cytoskeleton. Mol Biol Cell 15, 1197–1210.
Rink J, Ghigo E, Kalaidzidis Y, Zerial M (2005). Rab conversion as a mechanism of progression from early to late endosomes. Cell 122, 735–749.
Roh HC, Collier S, Guthrie J, Robertson JD, Kornfeld K (2012). Lysosome-related organelles in intestinal cells are a zinc storage site in *C. elegans*. Cell Metab 15, 88–99.
Rojas AM, Fuentes G, Rausell A, Valencia A (2012). The Ras protein superfamily: evolutionary tree and role of conserved amino acids. J Cell Biol 196, 189–201.
Sadler KC, Amsterdam A, Soroka C, Boyer J, Hopkins N (2005). A genetic screen in zebrafish identifies the mutants vps18, nf2 and foie gras as models of liver disease. Development 132, 3561–3572.
Salazar G *et al.* (2006). BLOC-1 complex deficiency alters the targeting of adaptor protein complex-3 cargoes. Mol Biol Cell 17, 4014–4026.
Schonthaler HB, Fleisch VC, Biehlmaier O, Makhankov Y, Rinner O, Bahadori R, Geisler R, Schwarz H, Neuhauss SC, Dahm R (2008). The zebrafish mutant *lbk/vam6* resembles human multisystemic disorders caused by aberrant trafficking of endosomal vesicles. Development 135, 387–399.
Schroeder LK, Kremer S, Kramer MJ, Currie E, Kwan E, Watts JL, Lawrenson AL, Hermann GJ (2007). Function of the *Caenorhabditis elegans* ABC transporter PGP-2 in the biogenesis of a lysosome-related fat storage organelle. Mol Biol Cell 18, 995–1008.
Setty SR *et al.* (2007). BLOC-1 is required for cargo-specific sorting from vacuolar early endosomes toward lysosome-related organelles. Mol Biol Cell 18, 768–780.
Sevrioukov EA, He JP, Moghrabi N, Sunio A, Kramer H (1999). A role for the *deep orange* and *carnation* eye color genes in lysosomal delivery in *Drosophila*. Mol Cell 4, 479–486.
Simmer F, Moorman C, van der Linden AM, Kuijk E, van den Berghe PV, Kamath RS, Fraser AG, Ahringer J, Plasterk RH (2003). Genome-wide RNAi of *C. elegans* using the hypersensitive rrf-3 strain reveals novel gene functions. PLoS Biol 1, E12.
Simpson F, Peden AA, Christopoulou L, Robinson MS (1997). Characterization of the adaptor-related complex, AP-3. J Cell Biol 137, 835–845.
Sitaram A, Marks MS (2012). Mechanisms of protein delivery to melanosomes in pigment cells. Physiology (Bethesda) 27, 85–99.
Sohn EJ, Rojas-Pierce M, Pan S, Carter C, Serrano-Mislata A, Madueno F, Rojo E, Surpin M, Raikhel NV (2007). The shoot meristem identity gene TFL1 is involved in flower development and trafficking to the protein storage vacuole. Proc Natl Acad Sci USA 104, 18801–18806.
Solinger JA, Spang A (2013). Tethering complexes in the endocytic pathway: CORVET and HOPS. FEBS J 280, 2743–2757.
Sriram VS, Krishnan KS, Mayor S (2003). *deep-orange* and *carnation* define distinct stages in late endosomal biogenesis in *Drosophila melanogaster*. J Cell Biol 161, 593–607.
Stiernagle T (2006). Maintenance of *C. elegans*. Wormbook Feb 11:1–11.

Suzuki T *et al.* (2002). Hermansky-Pudlak syndrome is caused by mutations in HPS4, the human homolog of the mouse light-ear gene. Nat Genet 30, 321–324.

Tamura K, Ohbayashi N, Ishibashi K, Fukuda M (2011). Structure-function analysis of VPS9-ankyrin-repeat protein (Varp) in the trafficking of tyrosinase-related protein 1 in melanocytes. J Biol Chem 286, 7507–7521.

Theos AC *et al.* (2005). Functions of adaptor protein (AP)-3 and AP-1 in tyrosinase sorting from endosomes to melanosomes. Mol Biol Cell 16, 5356–5372.

Thomas JL, Vihtelic TS, denDekker AD, Willer G, Luo X, Murphy TR, Gregg RG, Hyde DR, Thummel R (2011). The loss of vacuolar protein sorting 11 (vps11) causes retinal pathogenesis in a vertebrate model of syndromic albinism. Invest Ophthalmol Vis Sci 52, 3119–3128.

Tochio H, Tsui MM, Banfield DK, Zhang M (2001). An autoinhibitory mechanism for nonsyntaxin SNARE proteins revealed by the structure of Ykt6p. Science 293, 698–702.

Treusch S, Knuth S, Slaugenhaupt SA, Goldin E, Grant BD, Fares H (2004). *Caenorhabditis elegans* functional orthologue of human protein h-mucolipin-1 is required for lysosome biogenesis. Proc Nat Acad Sci USA 13, 4483–4488.

Urban D *et al.* (2012). The VPS33B-binding protein VPS16B is required in megakaryocyte and platelet alpha-granule biogenesis. Blood 120, 5032–5040.

Vonderheit A, Helenius A (2005). Rab7 associates with early endosomes to mediate sorting and transport of Semliki forest virus to late endosomes. PLoS Biol 3, e233.

Wang CW, Stromhaug PE, Kauffman EJ, Weisman LS, Klionsky DJ (2003). Yeast homotypic vacuole fusion requires the Ccz1-Mon1 complex during the tethering/docking stage. J Cell Biol 163, 973–985.

Warner TS, Sinclair DA, Fitzpatrick KA, Singh M, Devlin RH, Honda BM (1998). The light gene of *Drosophila melanogaster* encodes a homologue of VPS41, a yeast gene involved in cellular-protein trafficking. Genome 41, 236–243.

Wasmeier C, Romao M, Plowright L, Bennett DC, Raposo G, Seabra MC (2006). Rab38 and Rab32 control post-Golgi trafficking of melanogenic enzymes. J Cell Biol 175, 271–281.

Wurmser AE, Sato TK, Emr SD (2000). New component of the vacuolar class C-Vps complex couples nucleotide exchange on the Ypt7 GTPase to SNARE-dependent docking and fusion. J Cell Biol 151, 551–562.

Xiao H, Chen D, Fang Z, Xu J, Sun X, Song S, Liu J, Yang C (2009). Lysosome biogenesis mediated by *vps-18* affects apoptotic cell degradation in *Caenorhabditis elegans*. Mol Biol Cell 20, 21–32.

Yatsu A, Ohbayashi N, Tamura K, Fukuda M (2013). Syntaxin-3 is required for melanosomal localization of Tyrp1 in melanocytes. J Invest Dermatol 133, 2237–2246.

Yousefian J, Troost T, Grawe F, Sasamura T, Fortini M, Klein T (2013). Dmon1 controls recruitment of Rab7 to maturing endosomes in *Drosophila*. J Cell Sci 126, 1583–1594.

Yu W, Lin J, Jin C, Xia B (2009). Solution structure of human zeta-COP: direct evidences for structural similarity between COP I and clathrin-adaptor coats. J Mol Biol 386, 903–912.

Yu X, Lu N, Zhou Z (2008). Phagocytic receptor CED-1 initiates a signaling pathway for degrading engulfed apoptotic cells. PLoS Biol 6, e61.

Zhang L, Yu K, Robert KW, DeBolt KM, Hong N, Tao JQ, Fukuda M, Fisher AB, Huang S (2011). Rab38 targets to lamellar bodies and normalizes their sizes in lung alveolar type II epithelial cells. Am J Physiol Lung Cell Mol Physiol 301, L461–L477.

Zhu GD, L'Hernault SW (2003). The *Caenorhabditis elegans* spe-39 gene is required for intracellular membrane reorganization during spermatogenesis. Genetics 165, 145–157.

Zhu GD, Salazar G, Zlatic SA, Fiza B, Doucette MM, Heilman CJ, Levey AI, Faundez V, L'Hernault SW (2009). SPE-39 family proteins interact with the HOPS complex and function in lysosomal delivery. Mol Biol Cell 20, 1223–1240.

Zlatic SA, Tornieri K, L'Hernault SW, Faundez V (2011a). Metazoan cell biology of the HOPS tethering complex. Cell Logist 1, 111–117.

Zlatic SA, Tornieri K, L'Hernault SW, Faundez V (2011b). Clathrin-dependent mechanisms modulate the subcellular distribution of class C Vps/HOPS tether subunits in polarized and nonpolarized cells. Mol Biol Cell 22, 1699–1715.